공학박사 학위논문

Measurement and simulation for component-related radiosensitivity of Presage dosimeter

Presage 선량계의 성분에 따른 방사선민감도 측정 및 전산모사

2022 년 8 월

서울대학교 융합과학기술대학원
융합과학부 방사선융합의생명 전공

Shama Nassir J Alghadhban

A Dissertation for the Degree Doctor of Philosophy

Measurement and simulation for component-related radiosensitivity of Presage dosimeter

Presage 선량계의 성분에 따른 방사선민감도 측정 및 전산모사

August 2022

Program in Biomedical Radiation Sciences
Department of Transdisciplinary Studies
Graduate School of Convergence Science and Technology
Seoul National University

Shama Nassir J Alghadhban

Presage 선량계의 성분에 따른 방사 선민감도 측정 및 전산모사

지도 교수 예 성 준

이 논문을 공학박사 학위논문으로 제출함
2022 년 8월

서울대학교 융합과학기술대학원
융합과학부 방사선융합의생명전공
샤마 나시르 알가드반

샤마의 공학박사 학위논문을 인준함
2022 년 8 월

위 원 장 이재규

부위원장 예성준

위 원 최희동

위 원 김정민

위 원 엄영랑

Measurement and simulation for component-related radiosensitivity of Presage dosimeter

by

Shama Nassir J Alghadhban

A dissertation submitted to the Department of Transdisciplinary Studies in partial fulfilment of the requirement for the degree of Doctor of Philosophy in Biomedical Radiation Sciences in the Graduate School of Convergence Science and Technology

Seoul National University
August 2022

Approved by the thesis committee:

Chair Jae Kyoo Lee

Vice Chair Sung-Joon Ye

Examiner Hee Dong Choi

Examiner Jeongmin kim

Examiner Young Rang Uhm

Abstract

Shama Nassir J Alghadhban

Program in Biomedical Radiation Sciences

Department of Transdisciplinary Studies

Graduate School of Convergence Science and Technology

Seoul National University

In dosimetry, a radiation dosimeter with high sensitivity, especially at low doses, is favorable since radiotherapy treatments use low doses per session. Additionally, tissue-equivalent characteristics are important so that correction factors are not necessary. Another factor to consider for radiation dosimeters is their ability to measure the three-dimensional (3D) dose to validate the treatment plans for advance treatment techniques that may involve high dose gradients to deliver the required dose. Such validation and quality assurance are absolutely crucial as without this there may be unwanted lethal radiation doses risking critical organs. Investigation of dosimeter formulas that could be used for different purposes has been an ongoing

area of research where developments are possible. Another approach that could be applied to enhance the delivered radiation dose while minimizing its application to surrounding organs at risk is to use high atomic number nanoparticles. Experimental investigation of a tissue-equivalent dosimeter loaded with such nanoparticles can provide detailed information about the possible dependency of radiation energy, dosimeter components and formulas, and the size effect and concentration of nanoparticles.

Hence, this study has three primary objectives. The first objective is to develop an ideal dosimeter with higher sensitivity and tissue-like equivalent characteristics. Formulas named F1 and F2 were created for this particular purpose. The second objective is to determine how two bromine-based radical initiators and the addition of two different solvent types to the PRESAGE® formula affect the radiological characteristics and dose sensitivity of the PRESAGE® dosimeter. Formulas named as F3, F4, F5, F6, and F7 were developed for this investigation. Tetrabromomethane (CBr_4) and 1,1,1,2-tetrabromoethane ($C_2H_2Br_4$) radical initiators up to 2 wt.% were used in the fabrication of seven distinct PRESAGE® dosimeters. The dosimeters received either 250 or 100-kVp X-ray radiation with a

dose range of 0 to 40 Gy. A spectrophotometer was used to detect changes in optical density before and after exposure. Furthermore, while the quantity of dimethyl sulfoxide (DMSO) was 2 wt.%, the radiological characteristics and sensitivity of PRESAGE® dosimeters were examined for varied concentrations of radical initiators and cyclohexanone. The relative depth doses in PRESAGE®/water and the energy dependence for different X-ray beams and cobalt-60 were studied using Monte Carlo methods.

The third objective is to assess the physical dose enhancement impact of high Z GNPs on PRESAGE® formulas fabricated in-house, irrespective of biological enhancement and to investigate their enhanced characteristics. Monte Carlo simulations were also conducted to compare the experimental results.

The results for the first objective showed that fabricated in-house PRESAGE® dosimeter formulas F1 and F2 reacted differently to radiation with formula F2 having improved sensitivity to radiation compared to the previously published PRESAGE® dosimeter formula named as MOD3 accompanied with tissue-equivalent characteristics. Also, Monte Carlo simulations of depth-dose response confirmed that formula F2 can be used in both kilo- and megavoltage beams without

the requirement for correction factors.

The results for the second objective showed that PRESAGE® dosimeter formulas can be constructed with different chemical components to obtain higher sensitives. For example, formula F5, which has dimethyl sulfoxide (DMSO) incorporated into its mixture, indicated an increase in sensitivity of 46% with only 1% increase in its effective atomic number compared to the non-DMSO formula. Monte Carlo simulations also showed that the formulas can be used in megavoltage beams without the need for dosimetric correction factors, while a correction is needed with kilovoltage beams. Moreover, formulas with tetrabromomethane as a radical initiator exhibited higher sensitivity than the 1,1,1,2-tetrabromoethane formulas.

The third objective was achieved by incorporating gold nanoparticles into the tissue-equivalent PRESAGE® dosimeter, which showed noticeable dose enhancement dependent on beam energies, GNP size and concentration, and PRESAGE® dosimeter formula. This investigation provided an understanding of the factors that could influence dose enhancement results, including the dependence on PRESAGE® formulas. Results indicated that the bromine-based PRESAGE® dosimeter presented much higher dose enhancement

factors (DEFs) than the chlorine ones.

Keywords: PRESAGE®, dosimetry, gold nanoparticles, radical initiator, dose enhancement, sensitivity enhancement
Student Number: 2015-30894

List of Tables

List of figures

Table of Contents

Chapter 1. Introduction

1.1. Introduction to radiotherapy

The leading cause of death of this century has been cancer; there were nearly 10 million deaths in 2020 globally according to the International Agency for Research on Cancer (IARC)[1]. Although medicine and technology are developing every year, there are still many challenges facing cancer treatments. This includes treatment modalities, late diagnostic and disease screening, individual patients responding to treatment differently, and side effects of cancer treatments that could cause the second occurrence of cancer.

The major types of cancer treatments include radiation therapy, surgery, and chemotherapy. Either one of these treatments is used or a combination of two types or more. Radiotherapy (also called external beam radiotherapy) can deliver high ionizing radiation in curative or palliative doses. Curative doses are planned by the oncologist with the intention of curing cancer while palliative doses are for pain control and the temporary reduction of side effects.

Neutral or charged particles can be used to deliver deposited energy in a radiotherapy modality. In radiation therapy, there are three main photon interactions with matter; the photoelectric effect, Compton scattering and pair production.

These interactions deposit energy in a medium and the quantity of

deposited energy depends on the radiological properties of the medium, such as electron density, mass density, and atomic number (Z).

When an incoming photon interacts with a matter's inner orbital electron, photoelectric phenomena will occur; thus, the photon will transfer its energy to the electron, giving it enough energy to escape and be ejected, leaving a vacancy behind. Characteristic X-rays emissions can occur when the vacancy is filled by an outer electron and the production of monoenergetic Auger electrons can also occur when the characteristics X-rays are absorbed internally [2]. The mass photoelectric attenuation coefficient is proportional to Z^3/E^3, whereas Z is the atomic number of the medium and E is the photon energy [2]. From this relationship, it is well known that photoelectric effects are more pronounced at low photon energies and for high Z materials. The photoelectric interaction scheme is shown in Figure 1 (a).

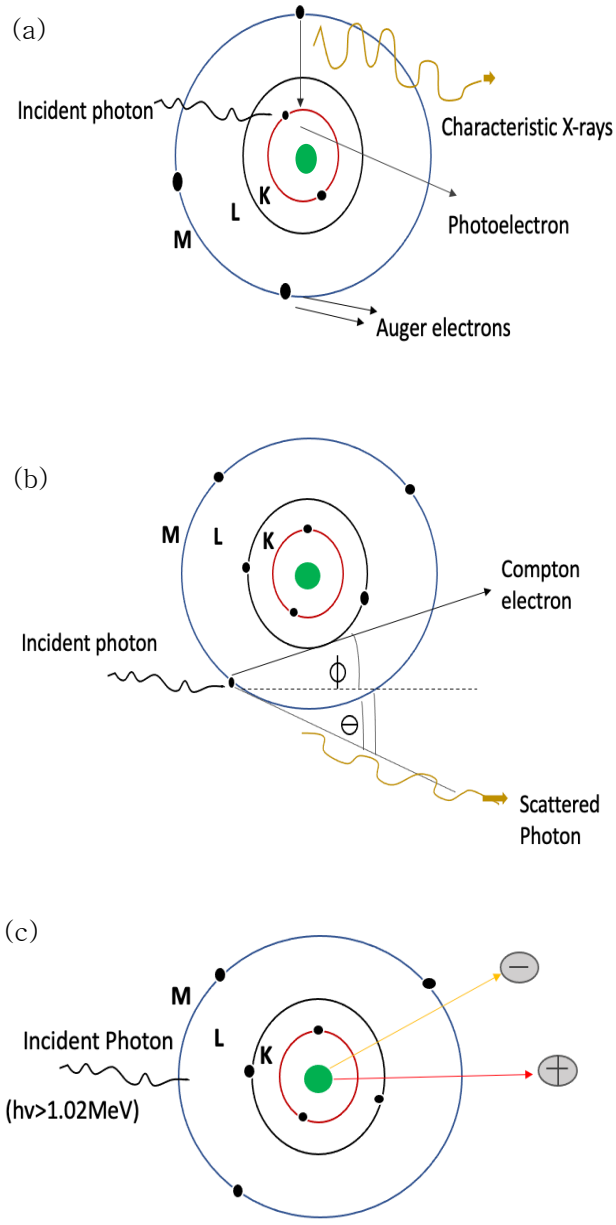

Figure 1. Diagram of photon interactions with matter: (a) photoelectric effects, (b) Compton scattering, and (c) pair production. Reproduced from [3].

The Compton scattering interaction, shown in Figure 1 (b), occurs when an incident photon interacts with loosely bonded electrons and, therefore, the photon transfers part of its kinetic energy to the electron. Thus, the electron will be ejected and the photon, with its remaining energy will be scattered. Compton scattering is dominant at high photon energies in the range that is usually used in radiation therapy [2]. The Compton scattering interaction is independent of the atomic number of the medium and rather depends on the number of electrons per gram of material [2].

Pair production interaction shown in Figure 1 (c), occurs when the incident photon has energy greater than 1.02 MeV (equivalent to the rest mass of two electrons). The process involves the absorption of the incident photon and the production of an electron and positron pair [2].

Additionally, the transmitted intensity, $I(x)$, of radiation that passes through a material of thickness (x) is defined as:

$$I(x) = I_0 e^{-\mu x}, \quad (1)$$

where I_0 is the intensity of the incident beam before attenuation and μ is the linear attenuation coefficient (cm^{-1}) (it depends on the photon energy and the atomic number of the material) [3]. Also, the mass-energy transfer coefficient μ_{tr} and the mass energy absorption

coefficient μ_{en}, can be used to express the energy that is attenuated or absorbed by the material [3].

Moreover, after photons interact with a medium, the generated electrons will further deposit their energy through Coulomb interactions. Those electrons are the primary cause of cell damage.

The ultimate purpose of radiation therapy is to deliver the prescribed dose to the tumor volume while minimizing its application to the surrounding organs. In order to achieve this with the best possible outcome for the patients, multiple factors can be modified, such as the energy of the incident beams and beam shielding, including multileaf collimation and customized blocks, beam angulation, beam flatting filters, wedge filters, compensators, breast cones, and a bolus. Therefore, advance radiotherapy treatment techniques have been progressed, such as three-dimensional (3D) conformal and stereotactic radiotherapy, volumetric modulated radiotherapy (VMAT), and intensity-modulated radiotherapy (IMRT). However, these techniques are considered susceptible to errors because they use very steep dose gradients to deliver the required dose [4]. As a result, 3D dosimeters (i.e., gels and PRESAGE®) have been invented to better analyze the absorbed dose and monitor possible errors that may come with such advance techniques and where conventional dosimeters

have difficulties determining the absorbed dose [5]. Nonetheless, adding gold nanoparticles to the medium can adjust the photon interactions and then increasing the dose to the tumor is possible.

1.2. Introduction to the PRESAGE® dosimeter

Solid-based dosimeters differ from gel-based dosimeters in that their mixture is comprised of synthetic plastic resins such as polyurethane. Plastic resins are made from liquid precursors that go hard over time as a result of polymerization reactions involving functional groups, such as alcohols and isocyanates in polyurethanes [6]. The PRESAGE® dosimeter is considered a solid-based dosimeter; it is an optically clear, solid polyurethane matrix comprised of a reporter component (i.e., leucomalachite green (LMG)) and a radical source (i.e., halocarbons) [7], [8]. The radiolysis of the radical initiator produces free radicals after irradiation, where the leuco dye is oxidized by the free radicals and result in a change in optical density (i.e., the color becomes darker) (Figure 2) [9], [10].

Radical initiators have weak covalent bonds with relatively low bond dissociation energies. Under specific conditions (such as radiation), the bond can split and free radical species are produced [11]. The proposed chemical scheme of the transformation from leucomalachite green (LMG) dye (colorless) to chromatic malachite green (its oxidized

Figure 2. PRESAGE® formula F2 fabricated in-house in a slab shape. The left side is not irradiated while the right side is irradiated with 5 Gy and 250-kVp X-rays. The color change due to radiation can be clearly seen.

product) is shown in Figure 3.

In summary, a transparent polyurethane plastic resin with a radical initiator acting as a source of radical species upon radiation and a leuco dye as acting as a reporter compound are the main chemical components that can be used to make a basic PRESAGE® dosimeter without characteristics improvement. Ultraviolet (UV) stabilizers can be added to the formula as an extra material to reduce the damage caused to the dosimeter by UV light [12]. Additionally, metal compounds such as dibutiltin dilaurate (DBTDL), can be added to the

PRESAGE® formula as a catalyst that can speed up the polymerization process between an isocyanate and a hydroxyl group of a polyol (to form polyurethanes) [13].

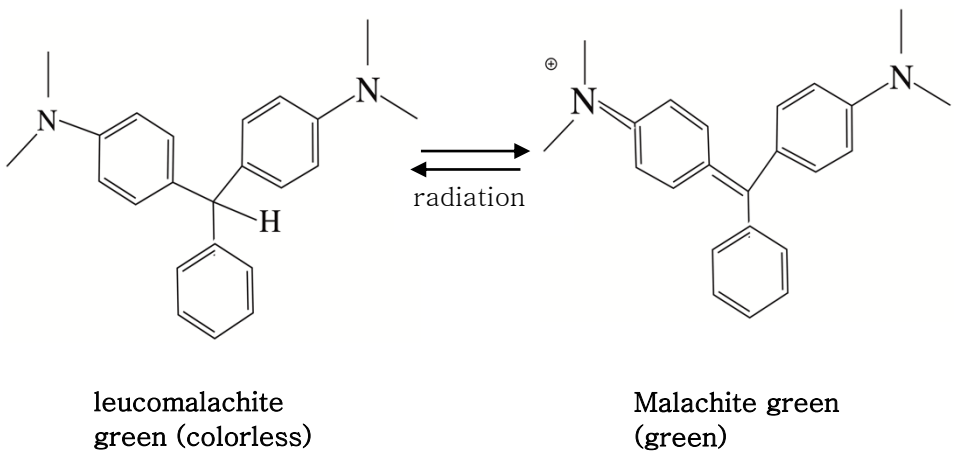

Figure 3. Proposed chemical scheme of the transformation from leucomalachite green (LMG) dye (colorless) to chromatic malachite green. Reproduced from reference [12].

1.3. PRESAGE® dosimeter in radiotherapy

Ionization chambers, diodes, thermoluminescent detectors (TLDs), and other conventional dosimeters with high precision are usually used in radiation oncology. However, they cannot measure the dose in three dimensions [14], which is particularly important for advance techniques that use steep dose gradients such as intensity-modulated radiation therapy (IMRT), volumetric arc therapy (VMAT), and stereotactic radiosurgery (SRS). Consequently, an important area of

study is the investigation of 3D dosimetry systems to assess absorbed dosage distributions [15], [16]. So, 3D gel dosimeters have been established and can be classified into two types: polymer gels and Fricke gels [17]. However, several polymer gel investigations have shown to contain severe problems, such as the requirement of supporting containers since the gel is not in a solid form [18], sensitivity to oxygen, and the dose distribution images having a diffusion [14], [15], [19].

Furthermore, the PRESAGE® dosimeter, which is a polyurethane-based radiochromic dosimeter with halogenated carbons acting as a free radical initiator and LMG acting as a radiation-sensitive reporter compound, was created to address these issues [7]. When irradiation hits the PRESAGE® dosimeter, the halogen-carbon bond produces free radicals, which oxidize the leuco dye and cause a color shift (optical density) [18]. PRESAGE® also has the benefit of being able to be designed and sculpted to meet the needs of diverse dosimetry applications.

The concentration and kind of radical initiator utilized in PRESAGE® manufacturing has no influence on post-irradiation temporal stability for over 168 h, according to reported studies [18]. However, increasing the quantity of radical initiator to more than 10% by weight would result in instability in the post-irradiation temporal response

because excess radical initiator would continue to oxidize the leuco dye, even after irradiation [18]. It has also been claimed that the change in optical density for absorbed dose is linear and that the increase in sensitivity is linked to the free radical initiator's low halogen-carbon bond dissociation energy [18].

With energies of 145 kVp X-ray energy and a 6 MV photon beam for dose rate, and 6 MV, 10 MV, 18 MV photon beams, and 1.25 MeV photons from a ^{60}Co source for energy dependence, researchers evaluated the influence of energy and dose rate on the radiochromic response of the PRESAGE®. They discovered that PRESAGE® is energy and dose rate independent across the whole studied range [7].

Two-dimensional (2D) PRESAGE® sheets with different thicknesses (up to 3 mm) were fabricated and used for patient quality assurance as a dosimeter for the patient surface. The unique characteristics of PRESAGE® make it possible for it to be fabricated with flexibility and softness so that it can conform to patient skin [20]. Reading of the sheets can be done using a commercial high-resolution scanner, such as an Epson 11000XL, in a way similar to films with some consideration for factors such as light exposure [21]. Wang et al. [20] found that PRESAGE® in sheet form can deliver accurate relative-dose measurements, similar to films, and they showed temporal stability over the investigated period of time. The dosimeter also display a

linear response to radiation when measured 2 h post-irradiation and minor dose rate, angular, and energy dependencies [22]. Youkahana et al. [23] fabricated PRESAGE® sheets and read them using a CLARIOstar microplate reader that could be operated in the UV/VIS spectrophotometer mode and is capable of measuring light absorbance to investigate scanning feasibility. Their results indicated that depth-dose curves and beam profiles can be obtained with high resolution in 2D using a microplate reader for the sheets, which were irradiated with megavoltage X-ray beams. Their results were also within experimental uncertainties compared to ionization chamber measurements. Moreover, Collins et al. [24] investigated reusable PRESAGE® sheets as an economical replacement of films or as a radiochromic patient bolus. They found that the sheets can be reused up to six times with a decay time of up to 24 h post-irradiation. They also concluded that the sheets are a promising alternative to films and have multipurpose use as a bolus [24]. Furthermore, Annabell et al. [25] used a PRESAGE® dosimeter to measure the peak-to-valley dose ratio (PVDR) for a microbeam collimated synchrotron source. In their investigation they used confocal microscopy to evaluate the dose response of the PRESAGE® dosimeter, which provides higher resolution than optical computed tomography. Their results indicated the possibility of using PRESAGE® as a dosimeter with confocal

microscopy and the PVDR was estimated to be 52:1 at a depth of 2.5 mm, which was in a good agreement with EBT2 GAFchromic films and Monte Carlo simulations [25]. For clinical application, Rankine et al. [26] used cylindrical PRESAGE® 3D dosimeters to investigate the accuracy of image-guided radiation therapy (IGRT) for the treatment of small volumes delivered by a micro irradiator. Their results showed that PRESAGE® with an optical computed tomography (CT) readout system is a valid approach to verify small volumes when using IGRT. Moreover, Costa et al. [27] measured the response near the edges of 3D PRESAGE® dosimeters to investigate the electron return effect (ERE), which may happen at the tissue-air interface when using MR-linac for radiotherapy treatment instead of linac alone. Their investigation particularly involved the non-uniform response of dosimeter samples and a possible correction function for images. Their results indicated that higher sensitivity was observed near the edges (within 6 mm) and that only a partial correction function could be obtained; therefore, their recommendation was to remove the edges of the samples, resulting in uniform dose response [27]. Also, a PRESAGE® dosimeter was used as a dosimeter with a proton beam and their results indicated its possible use [28].

In summary, various publications regarding the PRESAGE® dosimeter indicate that it shows reliable behavior and can be used for different dosimetric purposes and applications.

Prior research has claimed that sensitivity may be adjusted based on the weight proportion of the radical initiator and the leuco dye used, though few investigations have demonstrated sensitivity variation dependent on the type of radical initiator and leuco dye material utilized [16]–[18], [29]. A small number of studies have been published comparing radical initiators with the same halogen atom and the impact of adding LMG solvents to the PRESAGE® formulation. Because some of the PRESAGE® components may be in powder or crystalline form, this inquiry is very useful in shortening the manufacturing process time [30].

Dimethyl sulfoxide (DMSO) is a polar aprotic solvent that is odorless, colorless, and hygroscopic [31], [32], and is also known to be miscible with water and other organic solvents. Cyclohexanone is a cyclic ketone composed of cyclohexane with a single oxo group and it functions as a human xenobiotic metabolite [33]. Cyclohexanone (known in organic synthesis) is considered a non-polar aprotic and colorless solvent that is also miscible with the majority of organic solvents [34]. It has been demonstrated that adding DMSO to a chemical formulation could increases dose sensitivity [35]. Also,

because dimethyl sulfoxide (DMSO) may operate as a “functional solvent,” providing both nanoparticle solvation and stabilization, it has been shown that this polar, aprotic molecule is a useful component for nanoparticle synthetization [36].

Previously, both DMSO and cyclohexanone solvents were utilized in the construction of PRESAGE® and gel dosimeters, either to improve dose sensitivity or to dissolve chemical reactants [35], [37], [38].

A water-equivalent dosimeter is preferable for clinical applications. To determine a dosimeter's water equivalency, its radiological properties must be calculated and compared to those of water [39]. This includes the calculations of mass density, effective atomic number, photon interaction probabilities (i.e., interactions cross sections), radiation dosimetry parameters (i.e., stopping power), the electron density of the materials (i.e., CT numbers), and relative dosimetry measurements (i.e., depth dose and output factors) [40]. Non-water-equivalent dosimeters, on the other hand, can be employed if dosimetric correction factors are applied to convert the recorded dose to an absorbed dose in water [19], [40]. Three innovative PRESAGE® dosimeters containing low amounts of metal compounds were developed and their sensitivity and water equivalency were tested by Alqathami et al. [15] . Results showed that all three formulas had better radiological water-equivalent qualities

than another previously published PRESAGE® formula [40]. This suggests that PRESAGE® formula qualities can be improved.

1.4. Gold nanoparticles in radiotherapy

In radiotherapy, maximizing the dose to the tumor tissue while minimizing it to the healthy tissue, where radiation passes through, has always been a huge challenge. Some techniques have been developed to compromise between the dose to the tumor and the accompanied side effects to the healthy tissue, such as enhancement of radiosensitization, increasing normal-cells tolerability to radiation, and reversing the radio-resistance behavior of tumor cells [41].

High Z materials have been proved to enhance the radiation dose when irradiated with kilovoltage X-rays (where the photoelectric effect is dominant and varies with Z^3) due to the increase in deposited energy from photoelectrons, characteristics X-rays, and short-range Auger electrons [42]. This increase is mainly concentrated to a tumor loaded with those high Z materials due to the production of low-energy Auger electrons, which typically deposit their energies in a distance range less than a micrometer [43].

Therefore, the importance of dose enhancement lies in the possible

reduction of prescribed radiation dosage and treatment sessions for radiation therapy. Gold nanoparticles (GNPs) (Z = 79) have higher mass-energy absorption coefficients than tissues and are one candidate to enhance radiation to tumors and act as a contrast agent for diagnostic imaging [44].

Some of the advantages of GNPs are their low systemic clearance, enhanced permeability and retention effects, biocompatibility, large surface-to-volume ratio such that drugs and agents can be attached to their surface, lower biological toxicity compared to traditionally used agents, such as the iodine agent for DNA-targeting, and can be synthesized in different diameters and as coating material [41].

GNPs can be manufactured to biologically target a particular type of tumor cell and can be delivered to them with the help of nanovectors, which simplify their tumor-cell uptake and, therefore, greater concentrations of GNPs can be seen in tumor cells rather than in healthy cells [45].

Several studies have reported the dose enhancement factors (DEFs) due to GNPs in vivo and in vitro for different GNP sizes, coatings, concentrations, and radiation sources [46]-[49].

The correlation between radiation exposure and the percentage of cells that survive is depicted by a cell survival curve. The clonogenic assay is a traditional technique for counting the number of cells that

retain their capacity to proliferate, even after being exposed to radiation. Single-cell suspensions of cells are used to prepare the assays before they are irradiated, frequently in conjunction with an agent; then the cells are seeded in culture dishes and left to grow for a number of weeks until observable colonies form [50]. The survival fraction can be calculated using $S = e^{-\alpha D-\beta D^2}$, where D is the delivered dose and α and β are fitting constants [51].

In vitro, Chithrani et al. [52] used a Hela cell line with a 1 nM concentration of 50 nm GNPs and irradiated it to 105 kVp and 6 MV. They reported radiosensitization enhancement factors (REFs) of 1.66 and 1.17 by examining the proteins γ-H2AX and 53BP1, which are linked to double-strand breaks (DSBs) locations. The measurement of DSBs utilizing foci at 4 and 24 h provided an estimate of remaining DSBs with and without treatment. Because γ-H2AX (not 53BP1) can be linked with apoptosis and chromatin compaction in early mitosis, thus the use of both indicators (γ-H2AX and 53BP1) allowed for direct comparison and colocalization [52]. This suggests that, for in-vitro studies and both lower and higher energies, clonogenic radiation cell survival is consistent with the rise of DSBs in cells with ingested GNPs [52]. Joh et al. [53] used the U251 cell line with 1 mM concentration of 12 nm GNPs and 150 kVp irradiation; a DEF of 1.3 was reported.

Also, different tumor models (EMT-6, Tu-2449, B16F10, etc.) were

studied in vivo with various radiation sources and the resulted effects included delay in tumor growth, 50% long-term survival and tumor growth inhibition [54]-[56].

Variations in reported results of DEFs have come from different GNP sizes and shapes, the cell line used, different coating materials, and different concentrations [43].

Furthermore, the exact mechanism of GNP radiosensitization has not been fully clarified. However, it was reported that total dose enhancement effects could include chemical and biological enhancements [57], not only the physical dose enhancement. This would explain the high DEFs calculated by the biological model of the cell line or tumors and what has been observed in MV irradiation (where Compton scattering is the dominant interaction and is independent of Z) [41], [58]-[60].

Those DEFs were higher and reported in kV irradiation, but lower factors in MV using Monte Carlo simulations have been reported where DEFs are based only on physical dose enhancement [41], [61]-[65].

It has also been reported that the generation of Reactive oxygen species (ROS) increases with smaller GNP size due to the higher surface-to-volume ratio and, therefore, the radiosensitization increases [42]. However, in vitro study using Hela cells, in comparison to GNPs 14 to 74 nm in size, showed those 50 nm in diameter had the

highest REF of 1.43 at 220 kVp compared to 1.20 and 1.26, respectively [52]. In another study with MAGICA polymer gel irradiated with 6 MV, they reported a maximum DEF for 50 nm GNPs when compared to 30 and 100 nm of 1.1, 1.17, and 1.12 [66].

On the other hand, it has also been shown that 50 nm GNPs have the maximum cellular uptake [67]. The struggle between the thermodynamic driving force for cell uptake and receptor diffusion kinetics leads to this size for the endocytosis process [52]. Unlike smaller GNPs, it was observed that 50 nm semiconductor nanoparticles can pass into the cells more effectively [68].

Our experimental and simulation investigations have demonstrated radiological and dose responses over a range of X-ray energies for seven in-house-made PRESAGE® dosimeters. Among these formulas, formulas F1 and F2 showed water-equivalent characteristics with improved sensitivity in F2 greater than that observed in a previously reported PRESAGE® formula named MOD3 [15]. It was also shown that F1 and F2 can both be used at kilo- and megavoltages without applying correction factors [30].

A limited number of previous studies have investigated the radiosensitization of GNPs incorporated into a PRESAGE® dosimeter [43], [69]. However, their reported DEFs results vary significantly.

The aim of this study is to investigate the radiosensitization of GNPs

incorporated into PRESAGE® dosimeters with the same halogen atom as the radical initiator and the effect of different PRESAGE® formulas on the calculated DEFs.

Thus, in this study, the dependence of radiosensitization on GNP concentration and size, and X-ray energy were comprehensively investigated using two tissue-equivalent PRESAGE® dosimeters (formulas F1 and F2) and Monte Carlo simulations.

In general, the first purpose of this research is to create a PRESAGE® dosimeter with enhanced sensitivity compared to previously published dosimeters with tissue-like equivalent characteristics. Two PRESAGE® dosimeters were fabricated in-house for this investigation. The second purpose of this research is to investigate the effect of using two types of solvents with two bromine-based radical initiators with five different fabricated in-house PRESAGE® formulas on radiological prosperities, post-irradiation temporal stability, and dose sensitivity of the dosimeters. As a result, PRESAGE® dosimeters with different weight percentages of radical initiators and solvents were manufactured in-house. To assess the sensitivity as a function of radiation doses, the absorption spectra of the PRESAGE® dosimeters were recorded. Each water equivalency of the PRESAGE® dosimeter was determined by calculating density, number of electrons per unit mass, electron density, mass-energy

absorption coefficients, effective atomic number, and relative depth doses.

The third purpose of this research is to investigate the dose enhancement factors (DEFs) for two PRESAGE® dosimeters fabricated in-house with GNPs. This investigation includes the dependency of the PRESAGE® formula, irradiation energies, GNP size effect, and GNP concentration.

Chapter 2. Materials and methods

2.1. PRESAGE® fabrication

2.1.a. Materials used for fabrication of formulas F1 and F2

The chemical substances employed in this investigation to create the PRESAGE® dosimeters are comprised of transparent polyurethane resin precursor (Crystal Clear 200, Smooth-On, Easton, PA USA), which comes in two parts: part A and part B. The radical initiators are tetrabromomethane (CBr_4) and 1,1,2,2-tetrabromoethane ($C_2H_2Br_4$), and the reporter compound is leucomalachite green (LMG). Cyclohexanone is used as a solvent and the catalyst dibutyltin dilaurate (DBTDL) was obtained from Sigma Aldrich (St. Louis, MO, USA) [70].

Firstly, the radical initiator was mixed with LMG dye. At this point, the solvent could be added to the mixture weather to optionally dissolve the LMG dye and make it cluster free or to dissolve the crystal-type radical initiator. It should be mentioned that LMG is in a white powder form and needs to be mixed for a long time until there are no observable clusters. If needed, a grinder could be used to smash the powder into smaller pieces, as shown in Figure 4 (a). Figure 4 (b) shows the LMG after dissolving it into the resin and adding solvent. With constant stirring, polyurethane resin precursor part A is then added slowly to the previous mixture.

Then, polyurethane resin precursor part B was added to the mixture and the mixture became denser; it takes around 20 min for the mixture to become solid. Lastly and as quickly as possible, DBTDL was added to the previous combination to increase sensitivity, polymerization, and post-irradiation stability [18]. Next, the PRESAGE® mixture was poured into polystyrene spectrophotometer cuvettes (inner dimensions of 1 cm × 1 cm × 4.5 cm and a wall thickness of 1 mm). These cuvettes next sat inside a pressure pot (60 psi) for 22 to 24 h to remove air bubbles that might impact dose

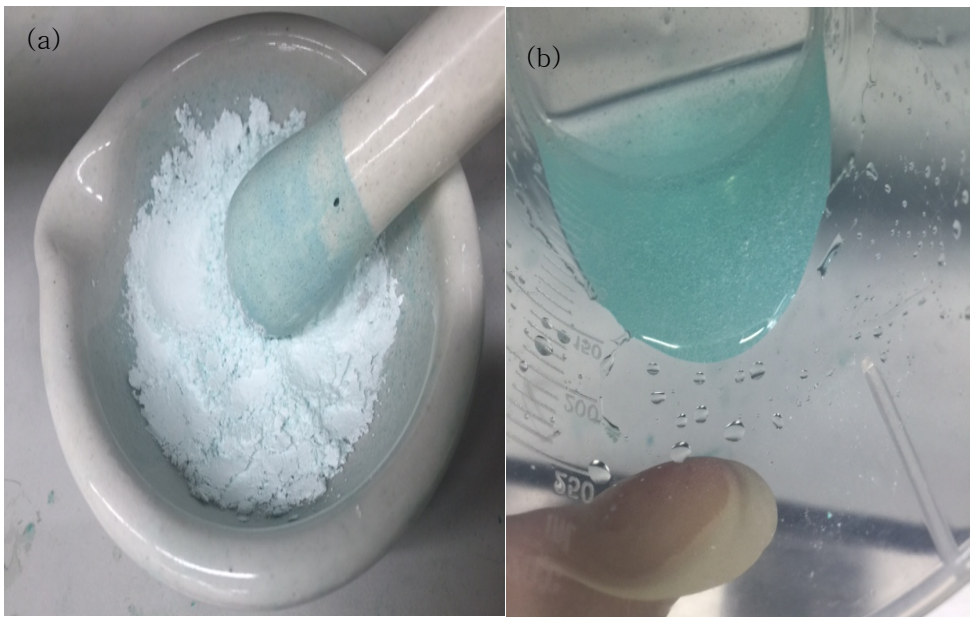

Figure 4. (a) Grinder that could be used to smash the LMG powder into smaller pieces, (b) Appearance of LMG after dissolving it into the resin (solvent can be added as well).

readings. Figure 5 shows the sequence of the general fabrication process and experimental setup of all PRESAGE® dosimeters.

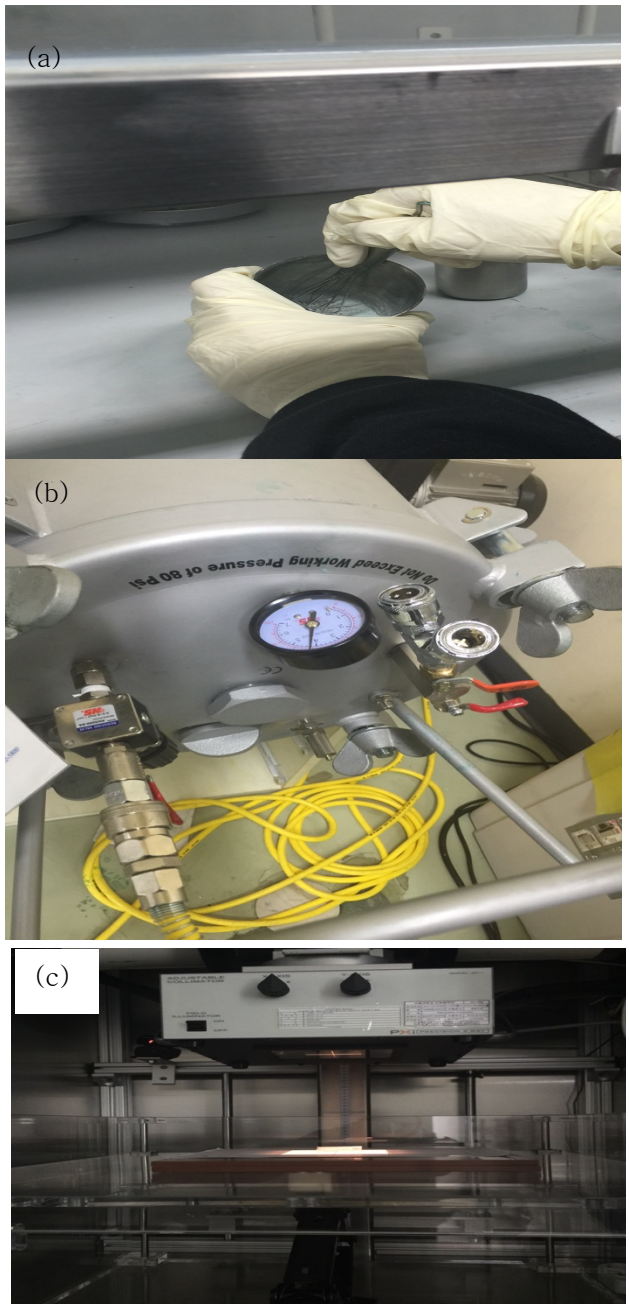

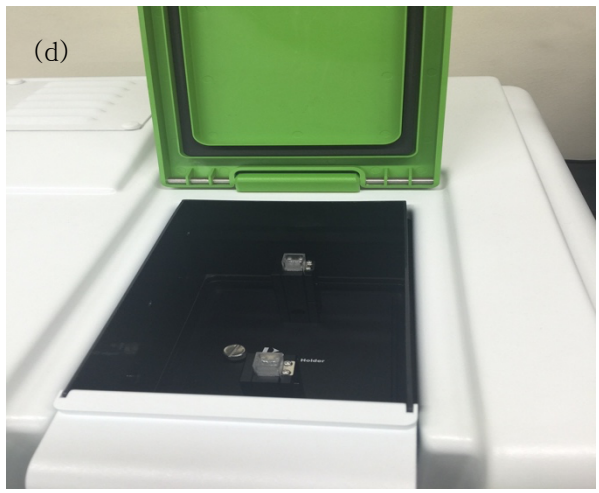

Figure 5. General experimental setup used in this study. (a) shows the first step of this experiment, which is dosimeter fabrication; (b) shows the second step, which involves placing the dosimeters into the pressure pot to eliminate any possible air formation. (c) shows the X-rad 320 (Precision X-ray, North Branford, CT, USA) used for KV samples irradiations. (d) shows the Ultraviolet/Visible spectrophotometer, which is used to measure the optical density of the sample pre- and post-irradiation.

2.1.b. Materials used for fabrication of formulas F3, F4, F5, F6, and F7

Similar fabrication processes and materials used in Section 2.1.a were used to fabricate F3, F4, F5, F6, and F7, with the addition of the two solvents cyclohexanone and DMSO (also acquired from Sigma Aldrich). However, different chemical weight percentages of the solvents were used.

2.1.c. Chemical formula

Various combinations of LMG solvents and initiators were created to examine the PRESAGE® dosimetry features (radiation sensitivity, linearity, and radiological properties). The amount of DBTDL is constant, i.e., 0.05 wt.%, within all formulas.

i. PRESAGE® formulas F1 and F2

Table 1 depicts the fabrication purpose of PRESAGE® dosimeters F1 and F2, as well as the varying weight percentages of the initiators, reporter compounds, and solvents employed in this investigation. Formula F1 was created by employing $C_2H_2Br_4$ as the radical initiator and adding solvent to provide tissue-like characteristics with increased sensitivity. While formula F2 accomplishes the same goal as F1, it employs CBr_4 as the radical initiator and a higher weight proportion of LMG with the added solvent.

Table 1. Two in-house made PRESAGE® dosimeter formulas with their fabrication purposes.

PRESAGE	Initiator wt.%	LMG wt.%	Solvent wt.%	Purpose
F1	$C_2H_2Br_4$ 0.55	2	Cyclohexanone 1%	trial for ideal formula with 1,1,2,2-tetrabromoethane radical initiator
F2	CBr_4 0.5	3	Cyclohexanone 4%	trial for ideal formula with tetrabromomethane radical initiator

ii.PRESAGE® formulas F3, F4, F5, F6, and F7

To achieve greater sensitivity, formula F3 was created with a comparatively high weight % of CBr_4. Formula F4 was created to compare the impact of adding two solvents, DMSO and cyclohexanone, to CBr_4. Formula F6, which is identical to F4 but has $C_2H_2Br_4$ as the radical initiator. Formula F5 was created to compare the effect of adding DMSO to formula F3 with formula F7, which is similar to F5 but has $C_2H_2Br_4$ as the radical initiator, instead of CBr_4. Table 2 displays the construction purpose of the five PRESAGE® dosimeters employed in this investigation, indicating varying weight percentages of initiators, reporter compounds, and solvents.

Table 2. Five different in-house made PRESAGE® dosimeter formulas and their fabrication purposes.

PRESAGE	Initiator wt.%	LMG wt.%	Solvent wt.%	Purpose
F3	CBr_4 2	2	Cyclohexanone 4%	highest amount of tetrabromomethane radical initiator
F4	CBr_4 1.5	2	Cyclohexanone 3%, DMSO 2%	the effect of adding solvent dimethyl sulfoxide "DMSO"
F5	CBr_4 2	2	Cyclohexanone 4%, DMSO 2%	the effect of adding solvent dimethyl sulfoxide "DMSO" to F3
F6	$C_2H_2Br_4$ 1.5	2	Cyclohexanone 3%, DMSO 2%	the effect of adding solvent dimethyl sulfoxide "DMSO" with 1,1,2,2-tetrabromoethane radical initiator
F7	$C_2H_2Br_4$ 2	2	Cyclohexanone 4%, DMSO 2%	the effect of adding solvent dimethyl sulfoxide "DMSO" with 1,1,2,2-tetrabromoethane radical initiator

2.1.d. Calculation of radiological properties

For each dosimeter, the elemental composition, electron density, effective atomic number, and the number of electrons per unit mass were computed. The Smooth-On crystal clear series was reported to have an elemental composition of 63.3% C, 9.4% H, 5% N, and 21.3% O [17]. The effective atomic number (Z_{eff}) was calculated from the Mayneord equation [2]:

$$Z_{eff} = \sqrt[2.94]{\sum_{i=1}^{n} a_i Z_i^{2.94}}, \quad (1)$$

where a_i is the relative electron fraction of the ith element and Z_i is the atomic number of each element. Electron density is defined as $\rho_e = N_e \times \rho$ (measured), where N_e is the number of electrons per unit mass and given as follows [71]:

$$N_e = N_A \frac{nZ_{eff}}{\sum_i n_i A_i} = N_A \frac{Z_{eff}}{\langle A \rangle}, \quad (2)$$

where N_A is the Avogadro's constant, A_i is the atomic mass of the i^{th} element and $\langle A \rangle$ is the average atomic mass of the compound [35]. Furthermore, by measuring the sample weight and volume at room temperature (22 °C), the mass densities of the PRESAGE® formulas was calculated [16].

2.1.e. Mass-energy absorption coefficient

For different PRESAGE® formulas, the mass-energy absorption coefficient (μ_{en}/ρ) can be used to determine water equivalency. Using the NIST XCOM X-ray attenuation database, the mass-energy absorption coefficient (μ_{en}/ρ) for a mixture was derived from equation (3) for each formula [72]:

$$(\mu_{en}/\rho)_{mixture} = \sum_i w_i \, (\mu_{en}/\rho)_i, \quad (3)$$

where w_i is the relative chemical weight of the i^{th} atom and $(\mu_{en}/\rho)_i$ is the mass-energy absorption coefficient for the i^{th} atom, which was obtained from the NIST database for each elemental composition.

2.1.f. Fabrication of PRESAGE® dosimeter with gold nanoparticles

The PRESAGE® dosimeters were fabricated using polyurethane resin precursor (Crystal Clear 200/204, Smooth-On, Easton, PA USA), bromine-based radical initiators, tetrabromomethane (CBr_4), 1,1,2,2-tetrabromoethane ($C_2H_2Br_4$), leucomalachite green (LMG) as the reporter compound, dibutyltin dilaurate (DBTDL) as the catalyst and cyclohexanone as the solvent. They were all acquired from Sigma Aldrich (St. Louis, MO, USA). CC 204 has a longer pot life than CC 200 (about 2 h compared to 20 min). Table 3 shows the weight percentage of each component, the elemental composition, and the fractional weight used to fabricate the control PRESAGE® dosimeters used in this study.

The gold nanoparticles used in this study were 50 nm gold nanospheres coated with polyvinylpyrrolidone (PVP) (nanoComposix, San Diego, CA, USA) and 5 nm gold 1-mercapto-(triethylene glycol) methyl ether functionalized nanoparticles (Nanoprobes, Inc. NY, USA).

Figure 6 shows the scanning electron microscope (SEM) images (7800F) for the 50 nm GNPs used in this study. The gold nanoparticles were incorporated into polyurethane resin precursor part B and sonicated for a minimum of 1 hr using an ultrasonicator vibra cell

(Sonics and materials Inc., Newtown, USA) or Branson 1800 ultrasonicator (Branson Ultrasonics Corporation, Danbury, CT, USA) [73]. With a relatively higher concentration such as 0.5 mM, the sonication time could be increased up to an extra 15 minutes. The concentrations chosen in this study were 0.125, 0.25, and 0.5 mM, which were lower than the reported [74] 50% lethal dose (LD50) that is equal to 5 g Au per kg for 11 nm GNPs injected into mice [43]. Such concentrations could be considered clinically relevant [75].

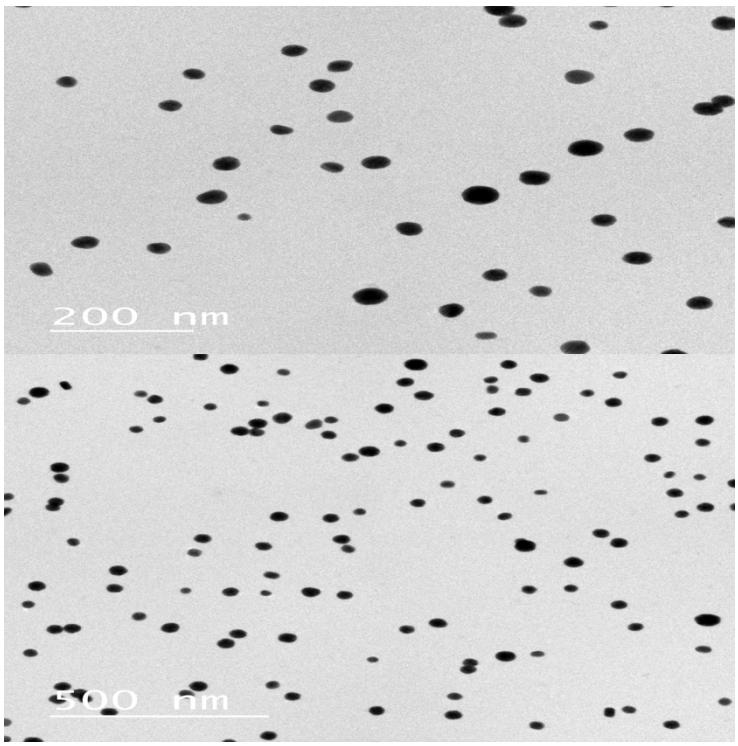

Figure 6. Scanning microscope images for 50 nm gold nanoparticles (GNPs) used in this study.

The radical initiator was mixed with the LMG dye and the solvent. Part A of the polyurethane resin precursor was increasingly added to this mixture with a continuous stir. Next, a combination of part B and the gold nanoparticles was added and mixed with the above mixture.

Finally, the catalyst DBTDL (0.05 wt.%) was added to the prior mixture, which was previously demonstrated to increase dose sensitivity, speed up the polymerization process, and reduce photofading after irradiation [69].

Subsequently, the PRESAGE® mixture was dispensed into polystyrene spectrophotometer cuvettes (inner dimensions of 1 cm × 1 cm × 4.5 cm with a wall thickness of 1 mm).

The resultant cuvettes were placed inside a pressure pot (60 psi) for 24–48 h to eliminate any possible formation of air bubbles that may affect dose measurements. Effective atomic number (Z_{eff}) was calculated using the Mayneord equation as an indicator of water equivalency.

PRESAGE® dosimeters F1 and F2 have a Z_{eff} close to that of water (7.417): 7.425 and 7.380 (0.1% higher and 0.5% lower than water, respectively). According to reports, the original previously launched PRESAGE® dosimeter had a 17 % higher Z_{eff} than water [19].

Table 3. Elemental composition, fractional weight (w_x), and weight percentage of control PRESAGE® dosimeters compared to water.

Material	W_C	W_H	W_N	W_O	W_{cl}	W_{Br}	W_{Sn}	Initiator wt. %	LMG wt. %	Solvent wt.% Cyclohexanone
Water	0.000	0.111	0.000	0.888	0.000	0.000	0.000			
F1	0.635	0.009	0.049	0.207	0.000	0.005	0.000	$C_2H_2Br_4$ 0.55	2	1
F2	0.640	0.009	0.048	0.203	0.000	0.004	0.000	CBr_4 0.5	3	4
Smooth-on crystal clear series[a]	0.633	0.009	0.050	0.213	0.000	0.000	0.000			

[a][16]

2.1.g. Dosimeters irradiation

i. Megavoltage beam irradiation

A linear accelerator (Elekta Synergy, Crawley, UK) from the St. Vincent's Hospital, Catholic University of Korea was used to for 6 MV irradiation. A major dose enhancement with 6 MV radiation is not expected since Compton scattering is the dominant interaction, however, measurements were made to differentiate between radiosensitization due to the GNPs and the possibility that the existence of GNPs could cause a chemical sensitivity change [43].

Cuvettes were irradiated to 1, 2, 5, and 10 Gy at a dose rate of 100 MU/Gy with the source to surface distance (SSD) of 100 cm from the

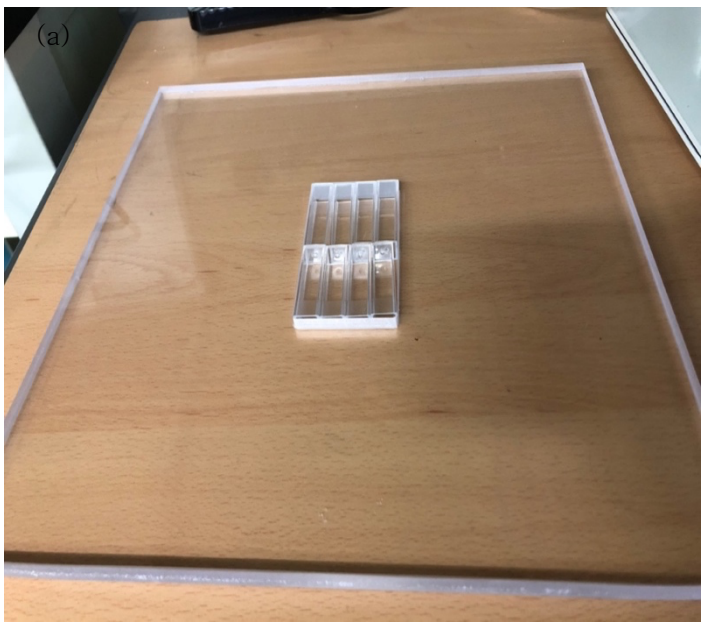

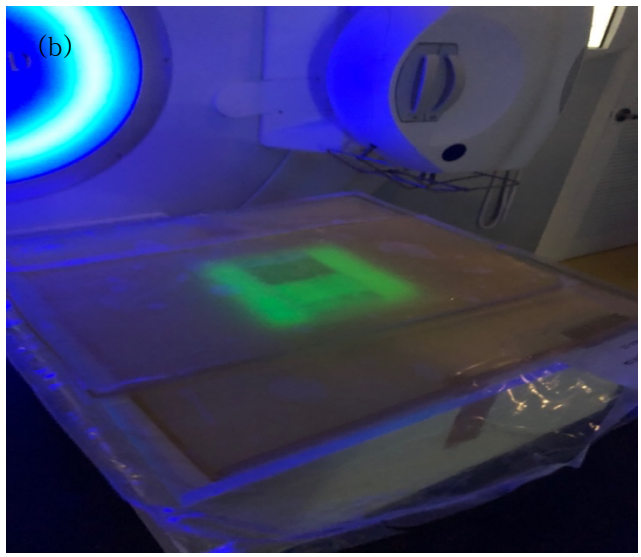

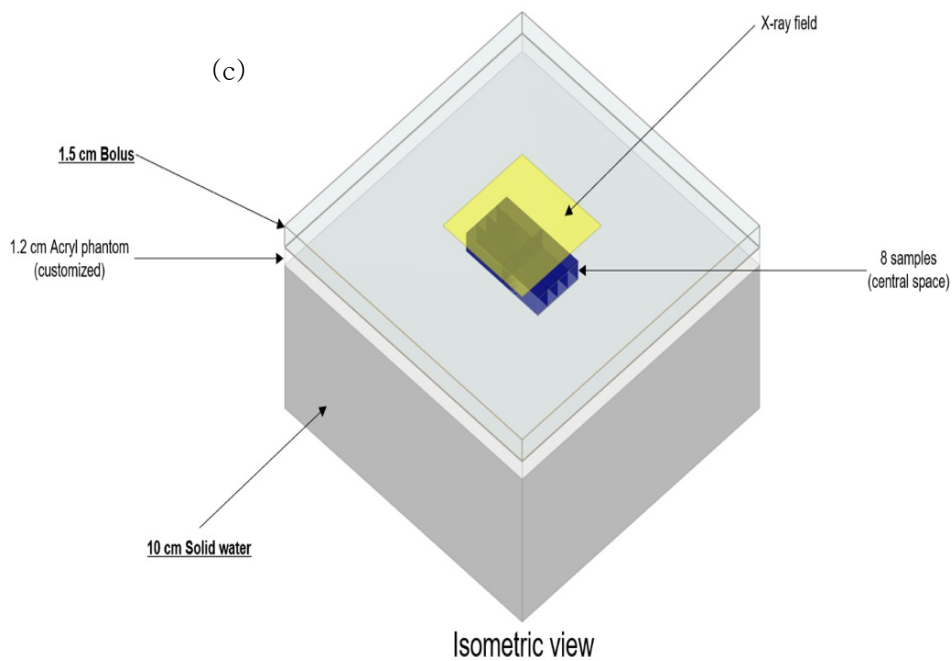

Figure 7. 6 MV irradiation setup using the Elekta linear accelerator as shown in (b) and (c); a customized acryl phantom was used to hold the cuvettes for uniform scatter conditions in (a).

source and a field size of 10×10 cm^2. A GNP concentration of 0.25 mM was incorporated into formulas F1 and F2 and chosen for the 6 MV radiation. The cuvettes were placed inside a customized acryl phantom and covered by a bolus to ensure uniform scattering conditions. Figure 7 shows the 6 MV irradiation setup.

ii. Kilovoltage beam irradiation

The PRESAGE® dosimeter cuvettes (which were fabricated in-house) were placed at 50 cm from the source and irradiated using an X-RAD 320 (Precision X-ray, North Branford, CT, USA). The cuvette is 1 cm × 1 cm × 4.5 cm in size. For the first and second objectives, the doses delivered to the cuvettes were 1, 2, 5, 10, 20, 30, and 40 Gy (for F1) with 250 kVp filtered by a 2 mm Al filter, 15 mA, and a 10 × 10 cm^2 field size (F1 at 100 kVp and 40 mA). For the third thesis objective, cuvettes were irradiated to 1, 2, 5, 10, and 20 Gy at 150 kVp, 15 mA, with a 2 mm Al filter and at an SSD 50 cm from the source with a 10 × 10 cm^2 field size.

2.1.h. Basic principle of spectrophotometry

A Lambda 365 UV/VIS spectrophotometer (PerkinElmer Inc., MA, USA) was used in this experiment. This system is capable of delivering

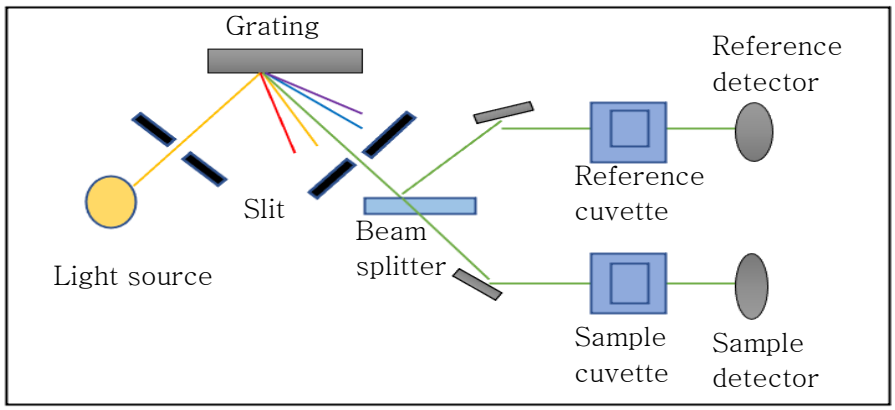

Figure 8. Basic components of the double-beam UV/VIS spectrophotometer. Reproduced from [94].

different spectral bandwidth, from 0.5 to 20 nm. Figure 8 shows the basic components of a double-beam spectrophotometer. Its main components include a light source, a slit, a grating, a beam splitter, two cuvette holders for a reference and a sample, and two detectors for the two cuvettes. The light source produces a light beam that passes through a slit (controls the light width and is usually in the range of ~1 nm) and then it hits a grating and a specific wavelength is selected. This light will irradiate the samples and the light intensity is detected [76]. Measurements using the double-beam spectrophotometer are done with the existence of a reference sample.

2.1.i. Optical absorption measurements

Absorbance spectra were obtained using a PerkinElmer Lambda 365 UV-VIS spectrophotometer (PerkinElmer Inc., MA, USA) with a wavelength range of 500 to 700 nm. The maximum absorption (λ) was discovered to be about 630 nm. The absorption of each PRESAGE® cuvette was measured before and after irradiation, and the difference was computed as Δ absorbance. The optical density is defined as the $\log_{10}$ of the ratio between the intensity of light passing through a sample (I) and the intensity of light passing though no sample (I_o): $\log_{10}(I/I_o)$ [43], [77]. It should be noted that the absorption spectra were measured using a reference cuvette (control) without irradiation from the same PRESAGE® batch. The reference absorbance was subtracted from the measured values. To avoid any absorbance changes due to UV or visible light exposure, all cuvettes were maintained in a freezer. Before the spectrophotometer measurements, samples were removed from the freezer and placed in a dark area for 2–3 h to enable them to rise to room temperature and pre-irradiation measurements were obtained. Within 1 hour after irradiation, measurements were acquired.

2.1.J. Monte Carlo modeling

i. Depth-dose simulation

For 50, 100, and 300-kVp X-ray beams and 1.25-MeV X-rays from cobalt-60, Monte Carlo simulations were performed to examine depth dosage differences between PRESAGE® formulas F2, F3, F5, MOD3 [15], and water. The calculations were made using Monte Carlo N-Particle Version 6.1 (MCNP6.1)[78]. An airbox with dimensions of 12 cm × 12 cm × 12 cm and a dosimeter box inside it with dimensions 1 cm × 1 cm × 10 cm were filled with PRESAGE® or water material was designed. The TMESH tally 1 was used to determine the relative dose throughout the central axis of the dosimeter box in the depth direction, in 0.1 cm × 0.1 cm voxels of 0.4 cm thickness [79]. Figure 9 explains the simulation geometry. The source was considered to be a plane source and was positioned on the surface of the dosimeter box facing the depth direction. The photon energy cutoff was 1 keV. Each simulation was conducted with 1×10^8 histories which represent the number of source particles needed to execute the simulation. X-rays were filtered with 2 mm Al and extracted from the SpekCalc code [80]. The X-ray spectra used in the simulations are shown in Figure 10.

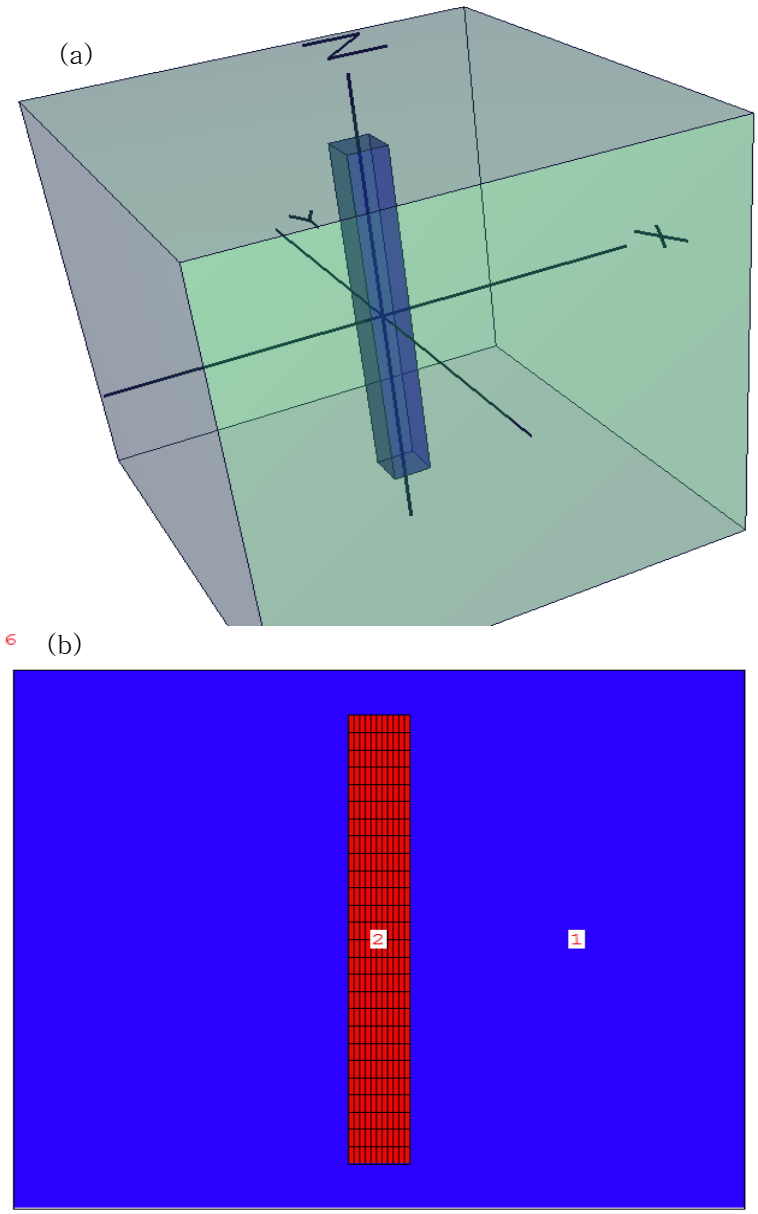

Figure 9. Geometry for Monte Carlo simulations; (a) shows the air box with the PRESAGE/water inner box and (b) shows the mesh tally and voxels structure used for this simulation.

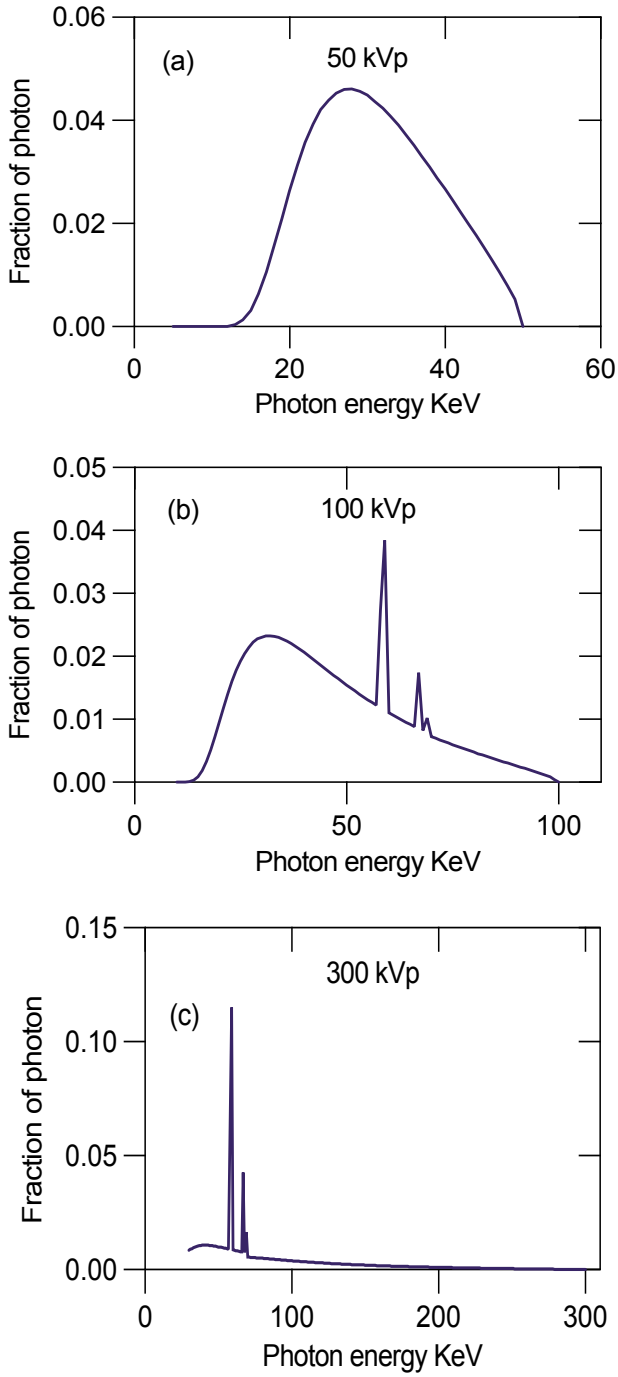

Figure 10. Incident X-ray source spectra for energies (a) 50 kVp, (b) 100 kVp, and (c) 300 kVp used in MCNP 6.1 simulations.

ii. Gold nanoparticles simulation

A Monte Carlo method was used to simulate PRESAGE® formulas F1 and F2 with different GNP concentrations used in the experiment for 150 kVp and 6 MV X-rays from LINAC. The calculations were made using Monte Carlo N-Particle Version 6.2 (MCNP6.2) [81].
For kV simulation, an airbox with 10 cm × 10 cm × 10 cm dimensions with a dosimeter cuvette inside having 1 cm × 1 cm × 4.5 cm dimensions and filled with PRESAGE® material with and without GNPs as a homogenous mixture was modeled.

Calculations of the relative dose across the central axis in a 1 cm depth direction (internal thickness of cuvette) of the dosimeter with and without the GNPs in 0.1 cm × 0.1 cm voxels of 0.1 cm thickness, was acquired using TMESH tally 1. The scoring volume was chosen to be in the middle of the cuvette (i.e., at a 0.5 cm depth). Figure 11 shows the geometry of the simulation.

The source was assumed to be as a plane source and was put on the surface of the PRESAGE® dosimeter, pointing in the depth direction. For the 6 MV simulation, the same geometry was used; however, an air box of 110 cm × 110 cm × 110 cm dimensions was used instead and the plane source was located at 100 SSD.

The photon and electron energy cutoff was 100 eV using the single-event transport method. This method allows simulation of individual

interactions down to the eV and can be chosen in the energy cutoff. Each simulation used 1×10^8 histories (the number of source particles to run the simulation).

The 150 kVp X-rays were filtered with a 2 mm Al filter and taken from the SpekCalc code [80]. The Elekta 6 MV photon spectra were obtained from [82]. Figure 12 shows the X-ray spectra used in the Monte Carlo simulations.

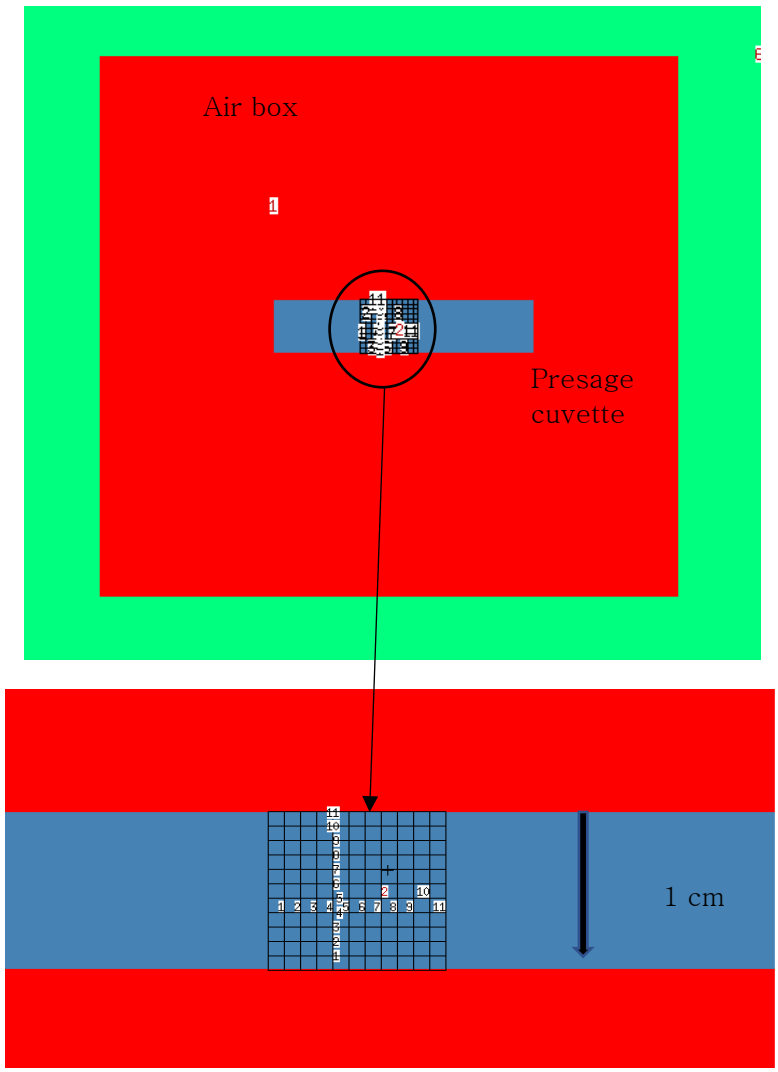

Figure 11. Monte Carlo simulation geometry used to acquire the energy deposition; the scoring volume is identified as 0.1 cm^3 and located in the middle of the cuvette (i.e., at a 0.5 cm depth) to mimic the spectrophotometer limited scoring volume.

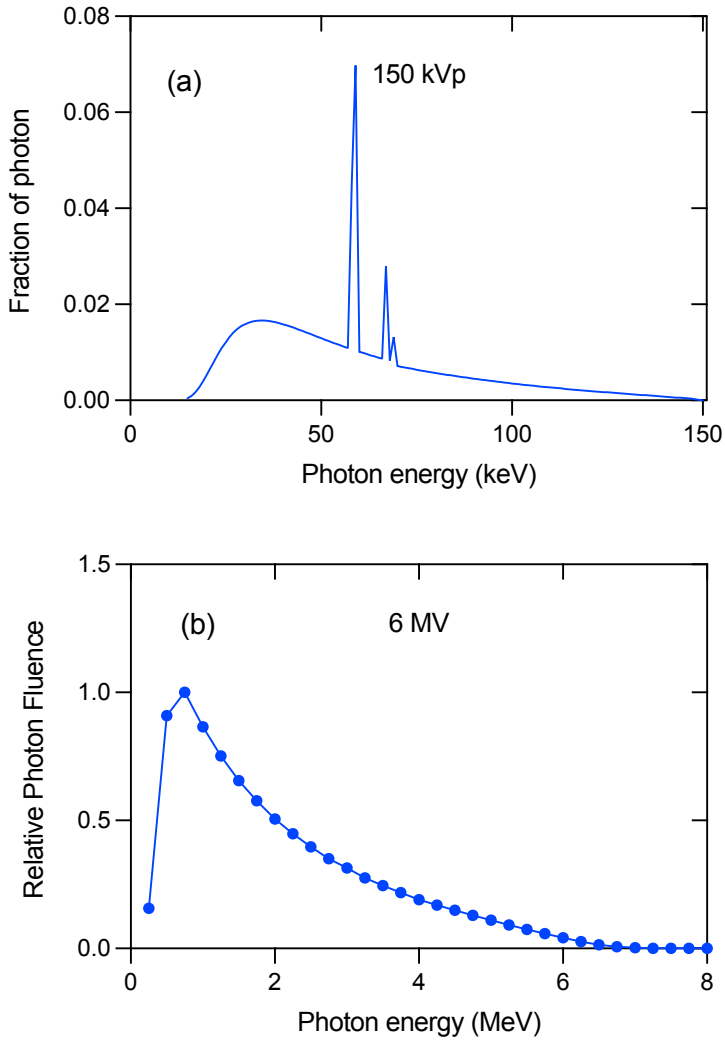

Figure 12. Incident X-ray source spectra for energies (a) 150 kVp and (b) 6 MV obtained from [82] and used in MCNP 6.2 simulations.

Chapter 3. Results and discussion

3.1. PRESAGE® dosimeter optimization of bromine-based radical initiators utilizing leucomalachite green and solvents①

3.1.a. Summary

The aims of this chapter were to first develop an ideal dosimeter with improved sensitivity and tissue-like equivalent characteristics. Secondly to determine how two bromine-based radical initiators, along with the addition of two different solvents to the PRESAGE® formula, affect the radiological characteristics and dose sensitivity of the PRESAGE® dosimeter. Seven distinct PRESAGE® dosimeters were created, each having up to 2% wt. of tetrabromomethane (CBr_4) or 1,1,1,2-tetrabromoethane ($C_2H_2Br_4$) radical initiators. They were exposed to either 250 or 100-kVp X-rays with doses ranging from 0 to 40 Gy. A spectrophotometer was used to quantify the changes in optical density before and after irradiation. Furthermore, the radiological characteristics and sensitivity of PRESAGE® dosimeters for various formulations were examined. The relative depth doses in F2, F3, F5 and water for 50, 100, and 300-kVp X-ray beams and 1.25

① "This article was published in Radiation Physics and Chemistry, vol. 194, S. Alghadhban et al., Optimization of bromine-based radical initiators using leucomalachite green and solvents in PRESAGE® dosimeter, 109985, Copyright Elsevier, May 2022."

MeV from cobalt-60 were calculated using Monte Carlo techniques. All PRESAGE® formulations showed a strong linear relationship between dose response and applied radiation dose. Even though the same weight percentage was used, CBr_4 demonstrated much greater sensitivity than $C_2H_2Br_4$. The F2 formula has higher radiation sensitivity than the MOD3 PRESAGE® dosimeter formula, as well as radiological qualities similar to water. If high sensitivity is necessary, the PRESAGE® dosimeters with CBr_4 as radical initiator can be employed. When a significant quantity of radical initiator (>0.50 wt.%) is used in the PRESAGE® formula, the effective atomic number is not water-equivalent. The inclusion of DMSO increased the sensitivity of the PRESAGE® formula F5 by 46.1%, with just a ~1% increase in the effective atomic number. In terms of simulated depth-dose response, PRESAGE® formula F2 was more similar to water than formulae F3 and F5, and hence may be employed in both kilovoltage and megavoltage beams without correction factors. The PRESAGE® dosimeters investigated showed good photostability over the examined time.

3.1.b. Radiological properties calculation

Table 4 presents the elemental composition for each dosimeter formulation and formula MOD3 [15]. Table 5 shows the measured and

computed effective atomic number, physical density, electron density, and the number of electrons per unit mass. Due to the smaller number of bromine-based radical initiators utilized in these formulations, the density of F1, F2, and F6 is closer to water, with variances of 6.1%, 5.8%, and 5.3%, respectively. Other formulae F3, F4, F6, and F7 have densities that are 12%, 11.6%, 13.5%, and 6.4% greater than water, respectively. The density changes can be attributed to the increasing amount of high atomic number elements employed in each formula, which were applied to increase the PRESAGE®'s sensitivity.

The computed electron densities of F1, F2, and F6 from the seven constructed formulas are only 2.9%, 3.0%, and 3.2% higher than that of water, respectively. Each PRESAGE® formula, from F1 to F7, has fewer numbers of electrons per gram than water by 2.0 %, 2.6 %, 2.9 %, 3.5%, 3.6%, 1.9%, and 1.4%, respectively. Z_{eff} in PRESAGE® dosimeters F1 and F2 is closest to water; Z_{eff} in F1 is only 0.1% higher, while Z_{eff} in F2 is 0.5% lower. Z_{eff} of the original PRESAGE® was observed to be 17 % higher than water [19].

When compared to the non-DMSO formula, the inclusion of DMSO solvent in F4 has little influence on the Z_{eff} (1.3% increase) (calculated for comparison). Similarly, F5 Z_{eff} rose by 1.1% when compared to non-DMSO formula F3. In general, as the concentration of the radical initiator employed in the formulas increases, Z_{eff} increases as well.

Table 4. Elemental composition and fractional weight (w_x) of PRESAGE® dosimeters and MOD3 compared to water.

Material	W_C	W_H	W_N	W_O	W_{cl}	W_{Br}	W_{Sn}	W_S
Water	0.0000	0.1119	0.0000	0.8881	0.0000	0.0000	0.0000	0.0000
F1	0.6350	0.0966	0.0499	0.2070	0.0000	0.0051	0.0001	0.0000
F2	0.6403	0.0935	0.0488	0.2035	0.0000	0.0048	0.0001	0.0000
F3	0.6293	0.0922	0.0477	0.2024	0.0000	0.0093	0.0001	0.0000
F4	0.6248	0.0923	0.0474	0.2038	0.0000	0.0045	0.0001	0.0082
F5	0.6228	0.0919	0.0467	0.2023	0.0000	0.0093	0.0001	0.0082
F6	0.6252	0.1013	0.0474	0.2038	0.0000	0.0039	0.0001	0.0082
F7	0.6234	0.1039	0.0467	0.2023	0.0000	0.0085	0.0001	0.0082
MOD3[a]	0.6259	0.0916	0.0494	0.2032	0.0284	0.0014	0.0001	0.0000
Smooth-on crystal clear series[b]	0.6330	0.0940	0.0500	0.2130	0.0000	0.0000	0.0000	0.0000

[a] [15]
[b] [16]

From Table 5, because of the increased mass density and atomic number of bromine in the radical initiator and other elements, such as tin, Z_{eff} of F3, F4, F5, F6, and F7 is greater than water by 28.8%, 22.1%, 30.2%, 20.4%, and 21.3%, respectively [83].

Despite the fact that the components of formulas F4 and F6 are equal in terms of weight percentage and differ in the kind of radical initiator (CBr_4 in F4 and $C_2H_2Br_4$ in F6), the Z_{eff} of F6 is 1.4% lower than that of F4. Likewise, for F5 and F7, the latter has 6.8% lower Z_{eff} than the former, demonstrating that formulas including $C_2H_2Br_4$ as the radical initiator have a lower Z_{eff} than formulas containing CBr_4. This is due to the fact that CBr_4 has a larger bromine content than $C_2H_2Br_4$. Using dosimetric correction factors, which may convert the measured dose to the absorbed dose in water, the water equivalency of the PRESAGE® dosimeter can be resolved [16], [19].

Table 5. Relative physical density (ρ), electron density (ρ_e), number of electrons per unit mass (n_e), and effective atomic numbers of the different PRESAGE® formulas used in this study and in MOD3, compared to water.

Material	ρ (g/cm^3)	ρ_e (10^{23} e cm^{-3})	n_e (10^{23} e g^{-1})	ρ_e (relative to water)	n_e (relative to water)	Z_{eff}
Water[a]	1.000	3.343	3.343	1.000	1.000	7.417
F1	1.061	3.442	3.273	1.030	0.980	7.425
F2	1.058	3.445	3.256	1.031	0.974	7.380
F3	1.120	3.576	3.247	1.070	0.972	9.553
F4	1.116	3.600	3.225	1.077	0.965	9.059
F5	1.135	3.658	3.222	1.095	0.964	9.657
F6	1.053	3.453	3.278	1.033	0.981	8.932
F7	1.064	3.506	3.294	1.049	0.986	8.998
MOD3[a]	1.044	3.421	3.277	1.023	0.980	7.416

[a] [15]

3.1.c. Determination of mass-energy absorption coefficient

Figure 13 illustrates the ratio of calculated mass-energy absorption coefficient (μ_{en}/ρ) between the seven formulas and water for photon energies ranging from 10 keV to 20 MeV. For all PRESAGE® formulas, a wide peak may be seen between 20 and 80 keV, with a drop down beyond 100 keV. The peaks appear at energies where photoelectric absorption is the most common photon interaction, which is affected by Z^3.

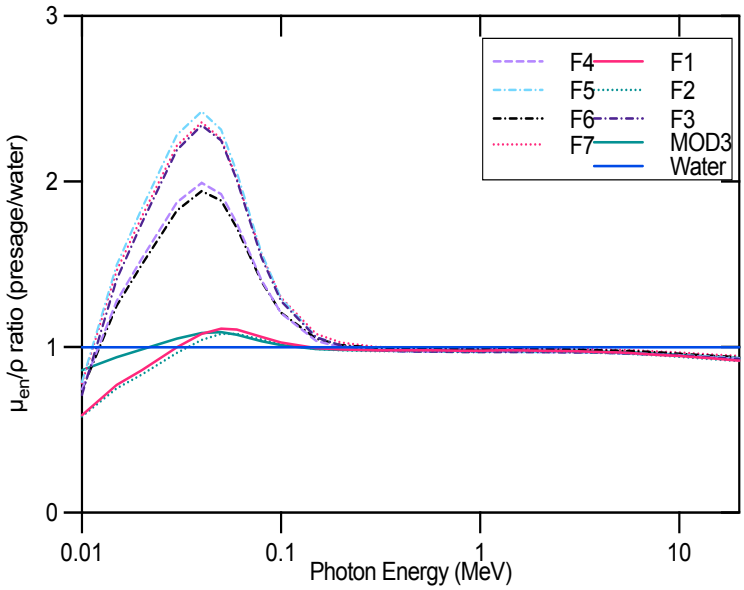

Figure 13. Mass-energy absorption coefficient ratios for all fabricated formulas and MOD3 relative to water as a function of photon energy.

The peak height is proportional to the fractional weight of bromine in the PRESAGE® formula (Table 4). Peaks corresponding to the formulas F1, F2, and MOD3 were roughly positioned at 50 KeV and were 11.0%, 8%, and 9% bigger than that of water, respectively. This was also observed in a previous study [84].

The peak for formulas F3, F4, F5, F6, and F7 was around 40 KeV, which is more than 50% higher than the peak for water. The ratios of all PRESAGE® formulas become approach one above 100 keV, when Compton scattering dominates. Their ratios are smaller than one above 3 MeV, when pair production becomes dominant. The fact that pair production is proportional to Z^2/A and water has a greater fractional weight of oxygen than synthetic PRESAGE® formulas, which have a higher fractional weight of carbon, and explains the difference in the ratio above 3 MeV [40].

3.1.d. Absorption spectrum

Figure 14 shows how different radiation doses affect the optical absorbance of PRESAGE® dosimeters. Figure 15 depicts the absorption spectra of PRESAGE® dosimeters recorded for formula F2 between the wavelengths of 500 and 700 nm.

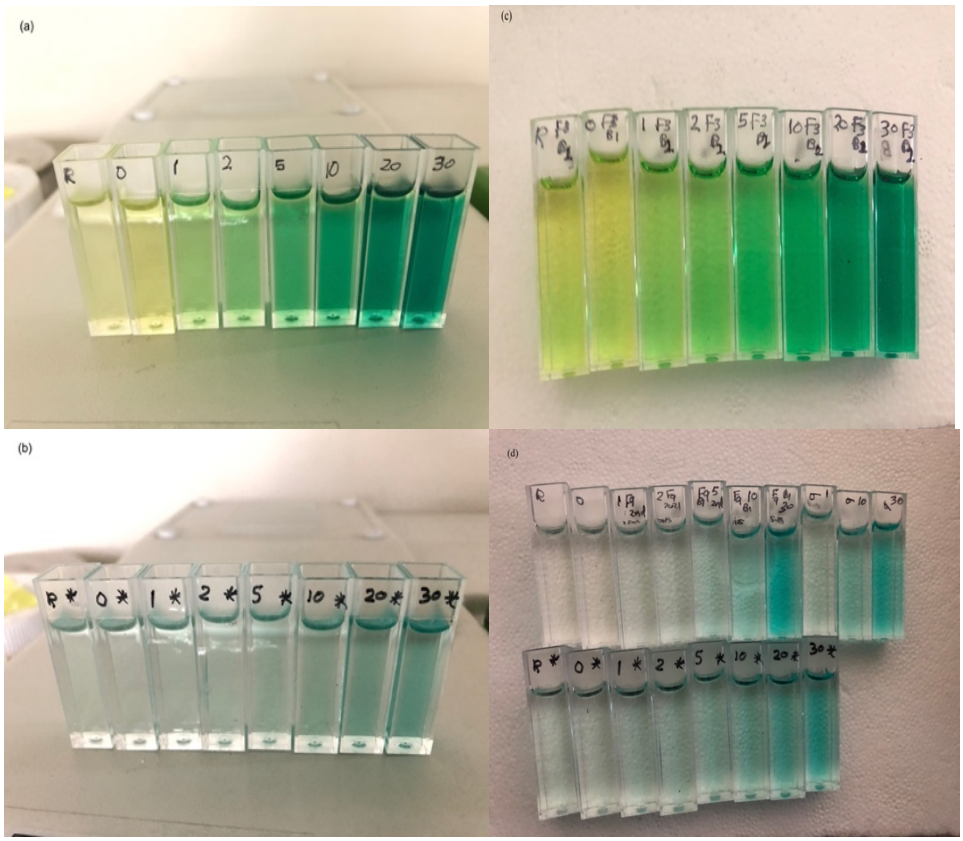

Figure 14. Formula F4 irradiated to 0, 1, 2, 5, 10, 20, and 30 Gy (R is the reference cuvette without irradiation) is shown in (a). Cuvettes for formula F7 irradiated to 1, 2, 5, 10, 20, and 30 Gy (R is the reference cuvette without irradiation) are shown in (b). Cuvettes irradiated to the same range of dose are shown in (c) for formula F3 and in (d) for formula F6. The color variances between the two PRESAGE® dosimeters are (a) and (c) yellow and in (b) and (d) blue is because of the different materials and weight percentages used in fabrication, such as a radical initiator, LMG, and cyclohexanone.

At around 630 nm, the highest absorption occurred. Peak intensities rose correspondingly with higher dosages, as can be shown. With the exception of F6 and F7, which displayed modest spectra changes at low doses (1 and 2 Gy) and as seen in Figure 16, all PRESAGE® dosimeters utilized in this investigation showed the same pattern.

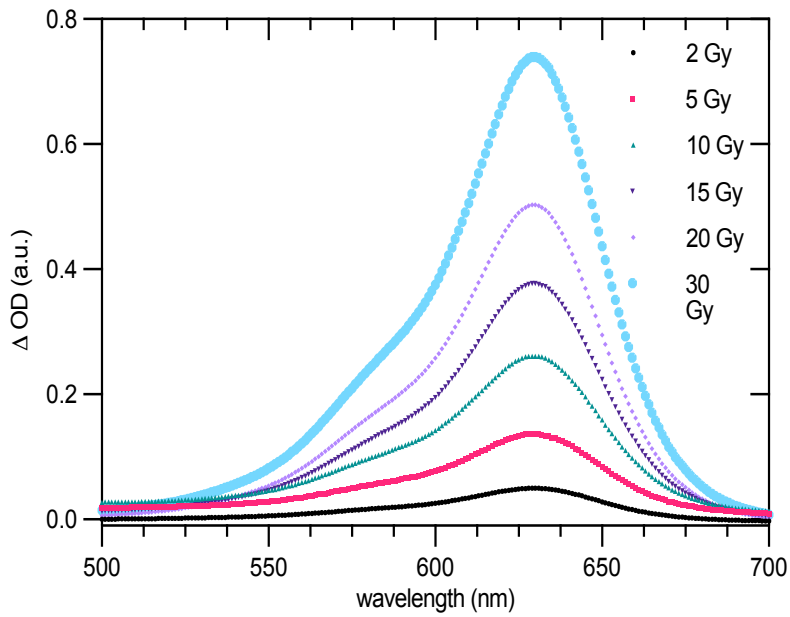

Figure 15. Absorption spectra of the PRESAGE® dosimeter formula F2 between 500–700 nm, showing absorbing maxima at around 630 nm after irradiation with multiple doses. The absorption was measured pre- and post-irradiation and the difference was calculated as Δ absorbance.

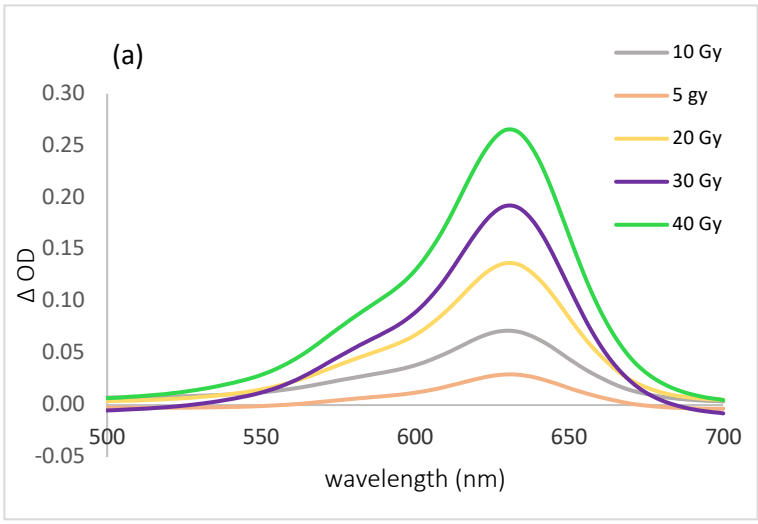
(a)
10 Gy
5 gy
20 Gy
30 Gy
40 Gy
0.30
0.25
0.20
0.15
0.10
0.05
0.00
-0.05
Δ OD
500
550
600
650
700
wavelength (nm)

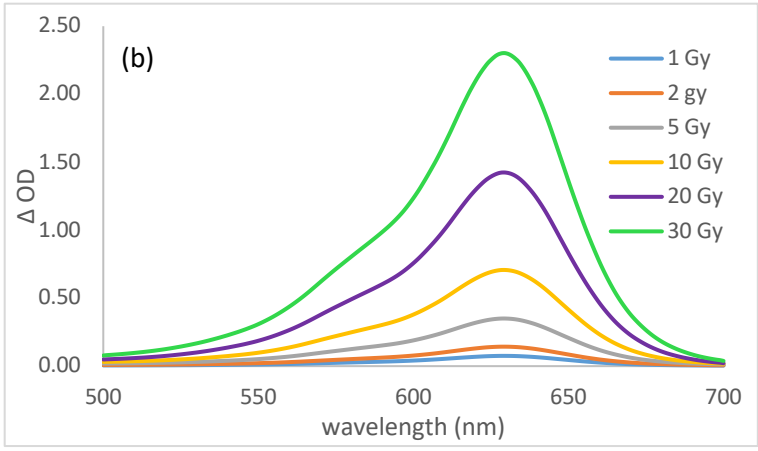
(b)
1 Gy
2 gy
5 Gy
10 Gy
20 Gy
30 Gy
2.50
2.00
1.50
1.00
0.50
0.00
Δ OD
500
550
600
650
700
wavelength (nm)

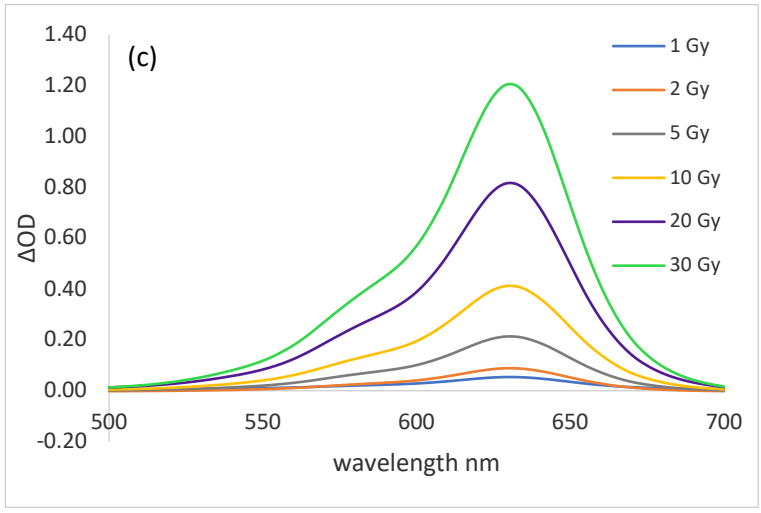
(c)
1 Gy
2 Gy
5 Gy
10 Gy
20 Gy
30 Gy
1.40
1.20
1.00
0.80
0.60
0.40
0.20
0.00
-0.20
ΔOD
500
550
600
650
700
wavelength nm

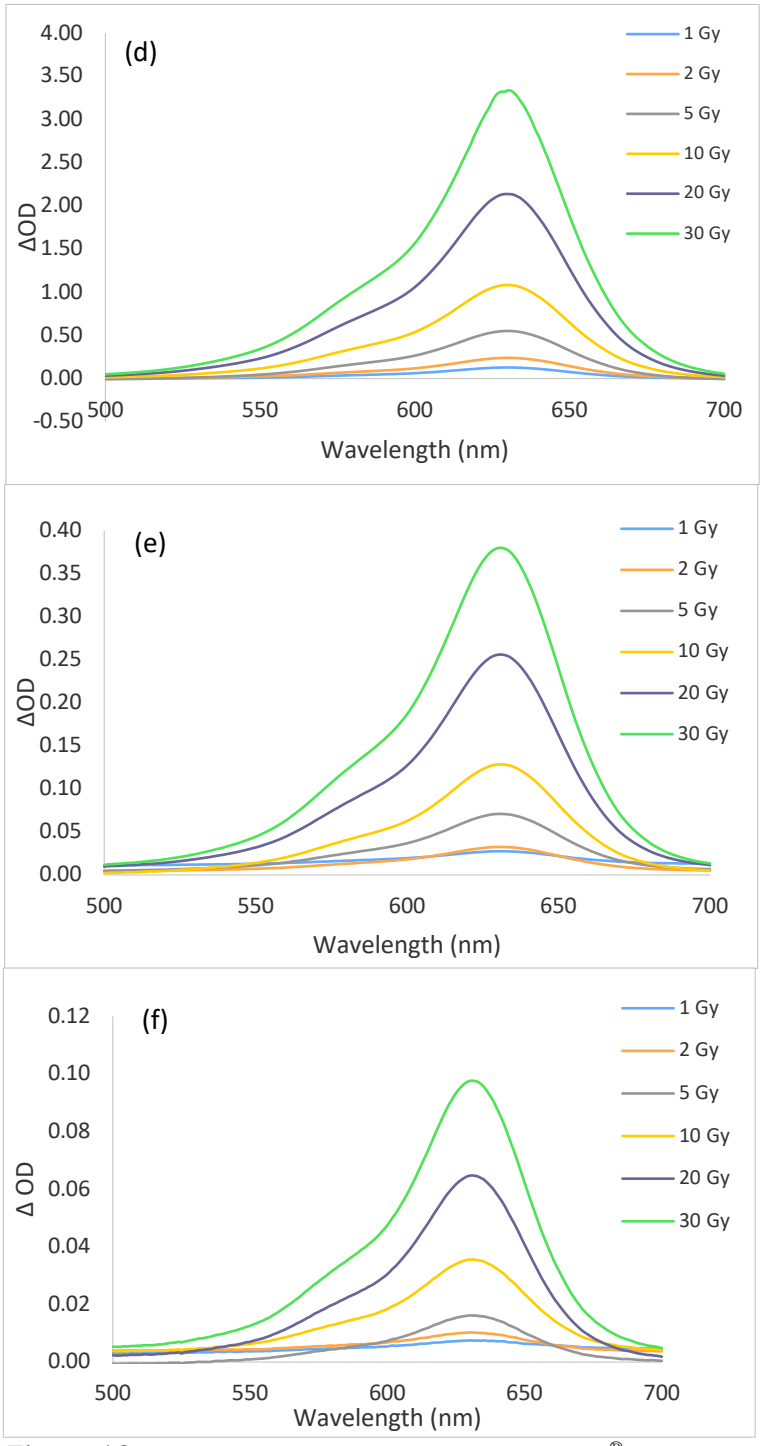

Figure 16. Absorption spectra of the PRESAGE® dosimeter formula (a) F1, (b) F3, (c) F4, (d) F5, (e) F6, and (f) F7 between 500–700 nm, showing absorbing maxima at around 630 nm after irradiation with multiple doses. The absorption was measured pre- and post-irradiation and the difference was calculated as Δ absorbance.

3.1.e. Calibration curve

For all of the dosimeters, Figure 17 depicts the variations in maximum absorbance observed versus absorbed doses. Over the examined radiation dosage range, all PRESAGE® formulas had a high linearity correlation ($R^2 > 0.99$). Figure 17 depicts the sensitivities and R^2 values for each of PRESAGE® dosimeters utilized in this investigation. The slope of the dose and absorbance in the optical density curve determine dose sensitivity [16].

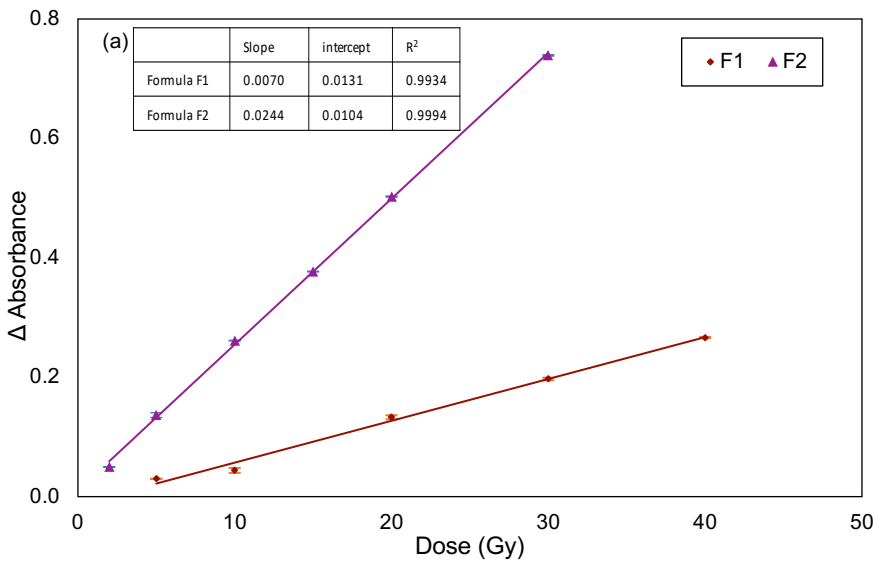

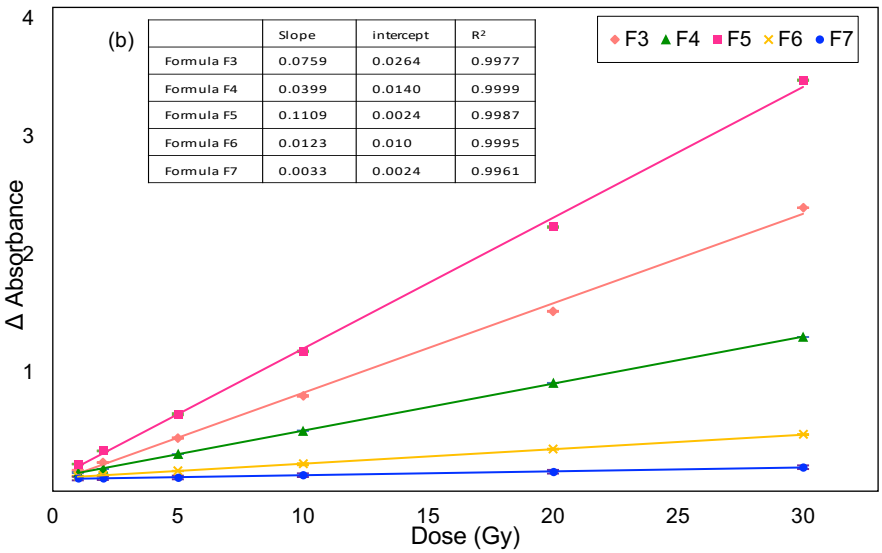

Figure 17. Absorbance changes as a function of absorbed radiation dose for (a) PRESAGE® formulas F1 and F2 and (b) formulas F3, F4, F5, F6, and F7, which were fabricated in-house, showing the response at 250 kVp within 1 hour after irradiation. Top left inset: correlation coefficient parameters, error bars: ± standard deviation (n = 3).

The results indicate that formula F2 has a higher sensitivity of 0.0244 Gy^{-1} compared to MOD3 [15], which has a sensitivity of 0.00722 Gy^{-1}. Z_{eff} is close to water in both F2 and MOD3 [15] with a 0.49% and 0.13% difference, respectively. Formula F5 has the highest sensitivity (0.1109 Gy^{-1}) of any formula and is 46.1% greater than F3 (without DMSO).

The inclusion of DMSO to the mix may be responsible for this rise. It was previously discovered that DMSO has a stabilizing effect on the initial and colored forms of malachite green derivatives, which adds to dose response. According to the PRESAGE® manufacturer (Heuris Inc.),

adding DMSO might boost sensitivity by 20 to 30%. [35], [37]. This observation might be noteworthy because adding DMSO to formula F5 enhanced its Z_{eff} by 1.1% when compared to formula F3.

Table 6 lists PRESAGE® formulas with cyclohexanone and DMSO as solvents, as well as their sensitivities and Z_{eff} values. The polyurethane resin used in the formulas listed in Table 6 was from the Smooth-On crystal clear series.

Formulas SS1 and SS2 [10] were developed to increase sensitivity and tissue equivalency. To boost their sensitivity, 7% cyclohexanone was employed with 0.25% bromotricholoromethane added in SS1. The higher solvent percentage compromises their tissue equivalency (Z_{eff} is 8.08 and 7.86) resulting in sensitivities of 0.0225 Gy^{-1} and 0.0213 Gy^{-1}. Formula MOD3 [15] was fabricated to have water-equivalent characteristics; chloroform and tetrabromoethane were used as radical initiators and Z_{eff} was 7.416 with lower sensitivity (0.0072 Gy^{-1}). In CC200 [85], a higher amount of tetrabromomethane (4%), DMSO (2%), and acetone (4.3%) were used to improve the sensitivity (0.0425 Gy^{-1}) but the Z_{eff} (11.1) was higher than all created formulas in this work. Formula CC200T [85] has the same components of CC200, however, 0.05% tartrazine (yellow dye No.5) was added to improve the sensitivity (0.0719 Gy^{-1}), Z_{eff}, on the other hand, was not altered (11.1). Formulas F3 and F5, instead, have higher sensitivity

and lower Z_{eff} 0.0759, 9.558 and 0.1109, 9.657, respectively (refer to Table 4 and Figure 17) [30].

Table 6. Studied PRESAGE® formulas with their names as they appeared in literature, sensitivity, and effective atomic numbers.

PRESAGE	Initiator wt.%	LMG wt.%	Other components wt.%	Sensitivity ΔOD/(cm.Gy)	Z_{eff}
SS1[a]	CBr4 0.50 CBrCl3 0.25	2	Cyclohexanone 7%	0.0225	8.08
SS2[a]	CBr_4 0.5	2	Cyclohexanone 7%	0.0213	7.86
MOD3[b]	$C_2H_2Br_4$ $CHCl_3$	2	-	0.0072	7.416
CC200[c]	CBr_4 4	2	DMSO 2% Acetone 4.3%	0.0425	11.1
CC200T[c]	CBr_4 4	2	DMSO 2% Acetone 4.3% Tartrazine 0.05%	0.0719	11.1

[a] [10]
[b] [15], refer to table 4 for elemental composition
[c] [85]

Figure 17 depicts the directly proportional association between increasing radical initiator, CBr_4 concentration, and dose sensitivity. When exposed to ionizing radiation, the quantity of free radical increases, causing additional oxidation of LMG and a significant rise in optical density change [15]. Also, formulas including CBr_4 as the radical initiator have greater sensitivity than formulas containing $C_2H_2Br_4$. CBr_4 has a slightly higher bromine percentage composition than $C_2H_2Br_4$, although it has a slightly lower molar mass (331.63 g mol^{-1}) than the latter (345.65 g mol^{-1}) (when dealing with the same weight of both initiators). This, however, does not explain the great sensitivity when CBr_4 is employed.

The use of cyclohexanone (LMG solvent) in PRESAGE® formulas had a significant benefit: it simplified and sped up the fabrication process, lowering the risk of fabrication mistakes and possible chemical toxicity. The effective atomic number was not tissue-equivalent in formulas F6 (1.5 wt.% $C_2H_2Br_4$) and F7 (2 wt.% $C_2H_2Br_4$), and the dosimeter's sensitivity was lowered by 73.1% in F7 compared to F6. However, with a large amount of CBr_4, the effective atomic number increased as the proportion of radical initiator increased, as did dosimeter sensitivity.

The sensitivity of the dosimeter is a significant aspect in dosimetry; a dosimeter with higher sensitivity is recommended, especially at low

radiation doses, where most treatments usually employ a dose of ~ 5 Gy [15].

3.1.f. Monte Carlo modeling

The Monte Carlo computed relative depth doses for the three PRESAGE® formulas and water using X-rays with energies of 50, 100, and 300 kVp and 1.25-MeV gamma rays from cobalt-60 are shown in Figure 18. In PRESAGE® formula F3 (Z_{eff} = 9.55) and F5 (Z_{eff} = 9.65), photoelectric absorption dominates at 50, 100, and 300 kVp, and the relative dose falls rapidly with depth. The attenuation behavior of Formula F2 (Z_{eff} = 7.38) and MOD3 (Z_{eff} = 7.416) is similar to that of water. As the energy grows, the disparity between relative doses decreases.

The relative depth-doses for the 50 kVp X-ray were 3.9%, 7.4%, 63.7%, and 66.5% lower than those for water, respectively. The relative depth dosage of formulas F2, MOD3, F3, and F5 at 5 cm depth for 1.25 MeV cobalt-60 gamma rays is only 0.61%, 0.33%, 1.5%, and 1.7% lower than water, respectively. This is owing to the lower atomic number dependence of Compton scattering (which dominates at high energy) [30].

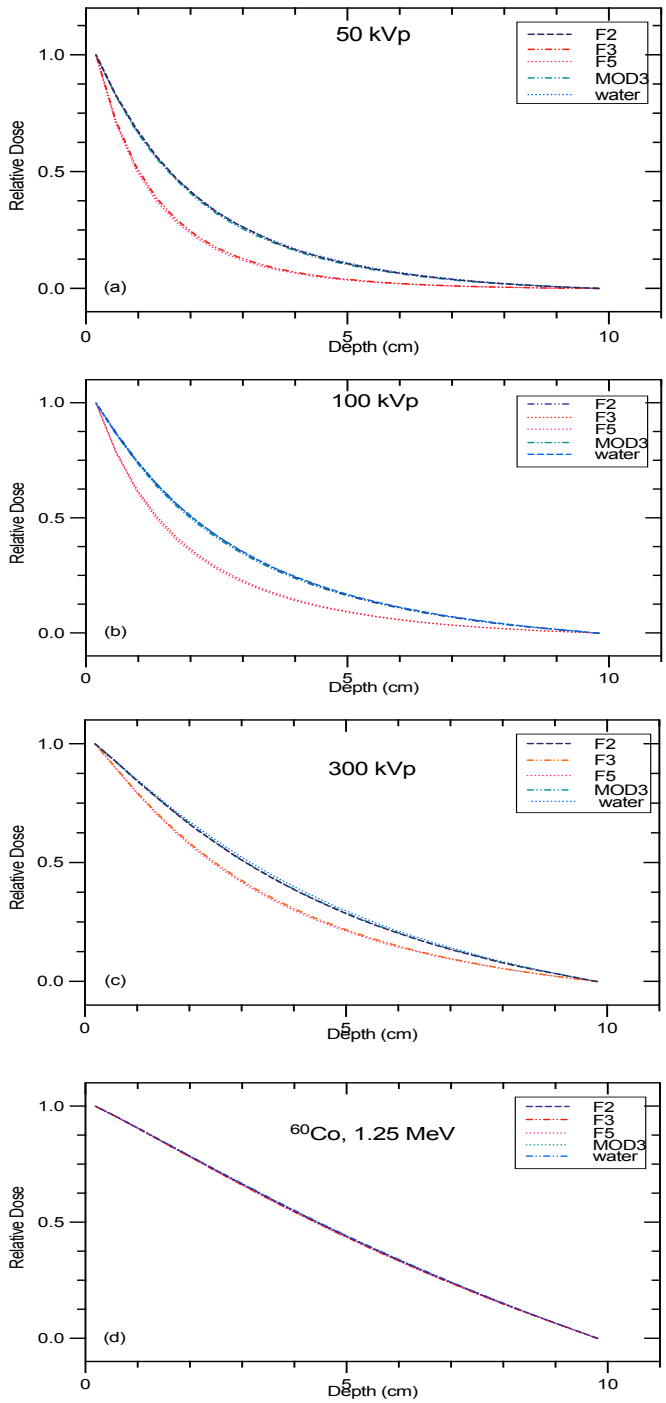

Figure 18. Monte Carlo simulation of the relative depth-dose curves for (a) 50 kVp, (b) 100 kVp, (c) 300 kVp, and (d) 1.25 MeV for the three PRESAGE® formulas and compared to MOD3 and water.

According to the depth-dose curves, PRESAGE® formula F2 is more water-equivalent than formulas F3 and F5 in terms of dose response for the four tested energies and may be utilized in both kilovoltage and megavoltage beams without the need for correction factors [30]. In the kilovoltage range, however, correction factors are necessary to convert the recorded dose to an absorbed dose in water using formulas F3 and F5.

Figure 19 indicates the map of energy deposited in the PRESAGE®/water box using the F8* tally and voxel mesh; higher energy deposition is seen near the surface of the box (at closer distance), which decreases with increasing depth.

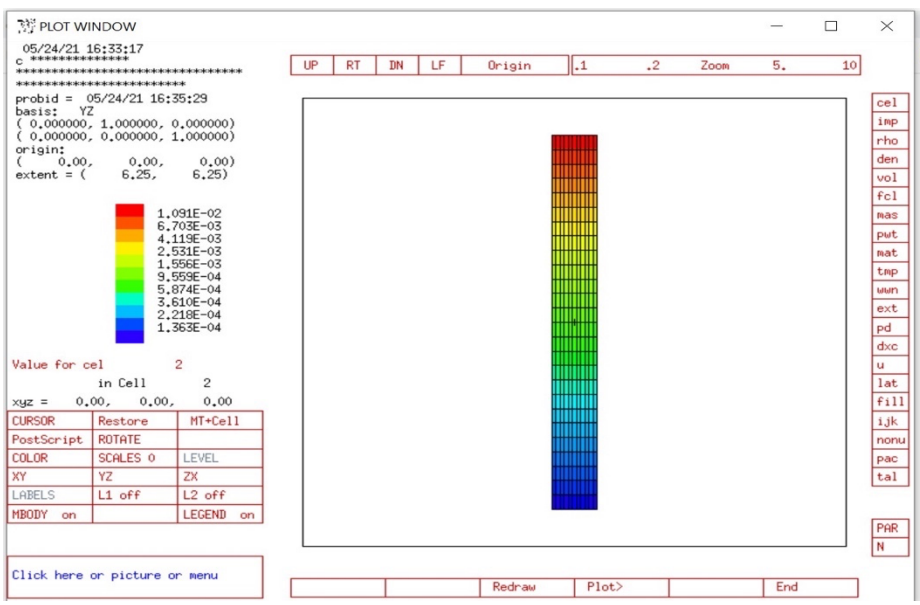

Figure 19. Energy deposition map inside the PRESAGE® box; the higher energy deposition is near the surface of the box and it decreases with depth, as indicated by red to blue color.

3.1.g. Post-irradiation photostability

The post-response stabilities of the seven formulas are shown in Figure 20. Figure 20 (a) demonstrates formulas with tertabromoethane as a radical initiator while (b) shows those with tetrabromomethane. The results reveal that the inclusion of DMSO or cyclohexanone in some of the formulas have no specific influence on the post-irradiation response photostability. Generally, all formulas showed stable behavior over the studied period.

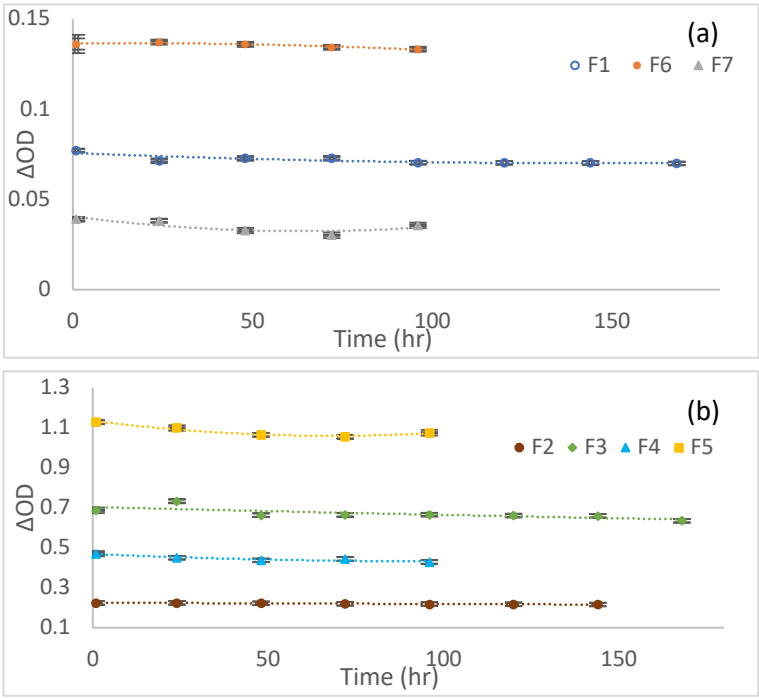

Figure 20. Photofading of PRESAGE® formulas over time: formulas with (a) tetrabromoethane as the radical initiator; and (b) tetrabromomethane as the radical initiator. Error bars: ± standard deviation.

It was found that dosimeters displayed 9%, 3.3%, 7.4%, 15.9%, 4.6%, 2.11%, and 8.7% photofading after the investigated post-irradiation time for formulas F1, F2, F3, F4, F5, F6, and F7, respectively. It has been said that adding a catalyst to PRESAGE® formulas would stabilize the lueco dye (i.e., LMG) by operating as singlet oxygen quenchers; where lueco dye bleach because of light is combined with the singlet oxygen [15].

Table 7. Inter-batch variability for three batches of each formula after exposure to 100-kVp X-rays.

Formula	Batch	ΔOD	SD
F1 (20 Gy)	1	0.133	0.00341
	2	0.141	0.00005
	3	0.149	0.00011
F2 (2 Gy)	1	0.051	0.00632
	2	0.050	0.00652
	3	0.052	0.00461
F3 (30 Gy)	1	2.328	0.00079
	2	2.302	0.00080
	3	2.266	0.00511
F4 (30 Gy)	1	1.206	0.00022
	2	1.192	0.00018
	3	1.183	0.00324
F5 (30 Gy)	1	3.389	0.00500
	2	3.383	0.00037
	3	3.208	0.00037
F6 (10 Gy)	1	0.136	0.00409
	2	0.138	0.00012
	3	0.144	0.00015
F7 (10 Gy)	1	0.039	0.00055
	2	0.036	0.00063
	3	0.036	0.00038

The inter-batch variability shown in Table 7 was determined for all formulas fabricated in-house. The difference tested to decide whether or not different batches of the same formula could be used for the same application.

3.1.h. Energy dependency

PRESAGE® formulas F2 and F5 were chosen for energy dependency investigation; F2 is water-equivalent with improved sensitivity while F5 has the highest sensitivity among the seven formulas and is not water-equivalent, their Z_{eff} values are 7.38 and 9.65, respectively. This investigation includes experimental and Monte Carlo simulations. PRESAGE® cuvettes were irradiated using an X-RAD 320 (Precision X-ray, North Branford, CT, USA) at 50 cm from the source. The doses delivered to the cuvettes were 5 and 10 Gy at 100 kVp and filtered by 2 mm Al, and 40 mA and 250 kVp filtered by 2 mm Al, 15 mA, with 10×10 cm^2 field size. Δ OD were then calculated and measured pre- and post-irradiation.

For the Monte Carlo simulation, calculations were made using Monte Carlo N-Particle Version 6.1 (MCNP6.1). An airbox with 10 cm $\times$ 10 cm $\times$ 10 cm dimensions and having a dosimeter cuvette inside it with dimensions of 1 cm $\times$ 1 cm $\times$ 4.5 cm that is filled with PRESAGE® or water material was modeled. F8* (energy deposition in a cell F8* tally (MeV)) was scored. The source was assumed as a plane source and placed on the surface of the dosimeter directed toward the cuvette. The photon energy cut-off was 1 keV. Each simulation was conducted with 1×10^8 histories and X-rays were filtered with 2 mm Al and

extracted from the SpekCalc code for 100 and 250 kVp [80]. Table 8 summarizes both experimental and simulation results.

Table 8. Summary of experimental and simulation results for energy dependency, error bars: ± standard deviation (n = 3) for experiment and relative errors in simulation.

Energy	Δ OD, expeirment		MCNP
F2, Z_{eff}= 7.380	5 Gy	10 Gy	energy deposition in a cell F8* tally (MeV)
100 kVp	0.1308 ± 0.00007	0.2781 ± 0.00022	7.95E-03 ± 0.0002
250 kVp	0.1365 ± 0.0040	0.2614 ± 0.00049	8.40E-03 ± 0.0002
% diff	4.1%	6.0%	5.8%
F5, Z_{eff}= 9.657	5 Gy	10 Gy	energy deposition in a cell F8* tally (MeV)
100 kVp	0.8823± 0.0015	1.7517 ± 0.0032	4.42E-03 ± 0.0003
250 kVp	0.6593 ± 0.0083	1.3486 ± 0.0060	3.07E-03 ± 0.0004
% diff	33.8%	29.9%	30.4%

Results showed an overresponse at 100 kVp compared to 250 kVp for formula F5 for both investigation methods. For the experiment and Δ OD readings for formula F5, an overresponse of 33.8% for 5 Gy and 29.9% for 10 Gy was seen at 100 and 250 kVp, respectively. Also, simulation results for formula F5 indicated an overresponse in energy deposition by 30.4% at 100 kVp compared to 250 kVp. On the other hand, formula F2 presented more energy-independent behavior at 100 and 250 kVp for 5 and 10 Gy; the difference was 4.1% and 6%, respectively, whereas the simulation results indicated a 5.8% difference between the two investigated energies (100 and 250 kVp).

Moreover, the results are in a good agreement with the ratio of mass-energy absorption coefficients as a function of photon energy shown in Figure 10, where formula F2 was closer to water at 100 keV and below other formulas with high atomic numbers, such as formula F5. Figure 21 shows the absorbance spectra acquired for formulas F2 (a) and F5 (b) using the low-energy 100 kVp at doses of 5 and 10 Gy.

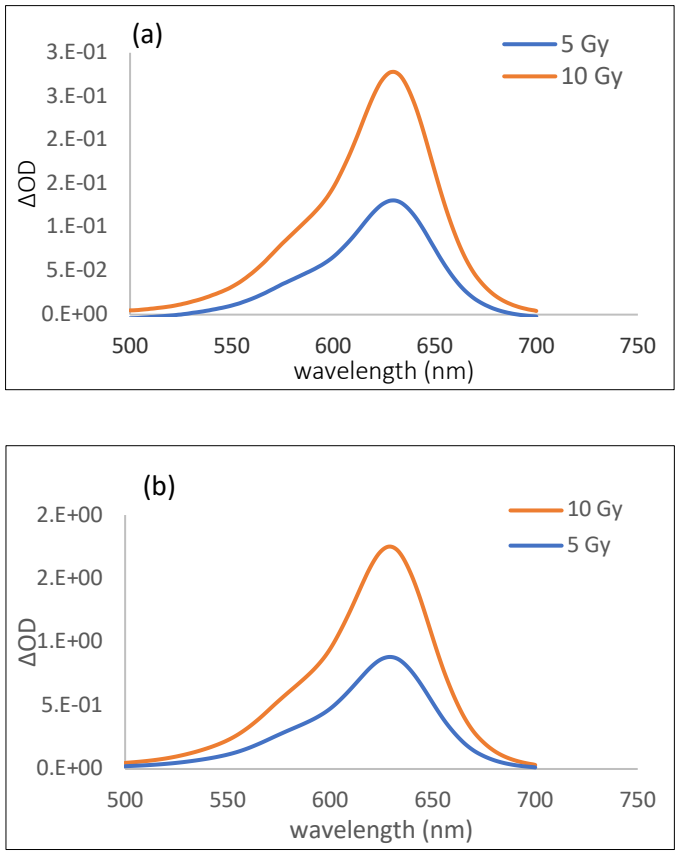

Figure 21. Absorbance spectra recorded between wavelength of 500 to 700 nm for formulas (a) F1 and (b) F5, showing an absorbance maxima at around 630 ± 3 nm after irradiating to 5 and 10 Gy and energy of 100 kVp.

3.2. Measuring X-ray dose enhancement by gold nanoparticles using two bromine-based PRESAGE® formulas

3.2.a. Summary

The aim of this study is to investigate the physical dose enhancement of two tissue-equivalent bromine-based PRESAGE® dosimeters fabricated in-house with the inclusion of gold nanoparticles. The dependency of dose enhancement factors on PRESAGE® formula, GNPs concentration and size, and irradiation energy are investigated.

Formulas F1 and F2 were fabricated for this purpose with tetrabromomethane (CBr_4) and 1,1,1,2-tetrabromoethane ($C_2H_2Br_4$) radical initiators. The dosimeters were irradiated with superficial 150 kVp and 6 MV X-ray beams. Their optical density changes pre- and post-irradiation with and without GNPs were measured using a spectrophotometer. DEFs for 0.125, 0.25, and 0.5 mM of 50 nm GNPs were calculated for both formulas. Also, DEFs were investigated for 0.25 mM 5 nm GNPs. Using Monte Carlo methods, DEFs were calculated and compared to experimental results.

Formulas with CBr_4 as the radical initiator showed higher DEFs than formulas with $C_2H_2Br_4$ when using the same 50 nm GNPs

concentrations of 0.25 and 0.5 mM. DEFs for formula F1 were 1.23, 1.26, and 1.27 and for formula F2 were 1.20, 1.33, and 1.45 for 0.125, 0.25, and 0.5 mM 50 nm GNPs, respectively.

6 MV irradiation indicated insignificant DEFs for both formulas with 0.25 mM of 50 nm GNPs, 4% and 2% for F1 and F2, respectively. The dose enhancement of 150 kVp at 0.25 mM of 5 nm GNP was 1.6 measured by F1, which implies the dependency of dose enhancement on GNP size. These results showed that dose enhancement is directly proportional to the GNP concentration used.

3.2.b. Absorption spectra

Figure 22 depicts the changes in optical absorption of PRESAGE® dosimeters with 0.0 0.125, 0.25, and 0.5 mM of GNPs. Absorption spectra irradiated to 10 Gy of PRESAGE® dosimeter formulas F1 and F2 measured between the wavelength of 500 and 700 nm are plotted in Figure 23. The maximum absorption was seen at approximately at 630 nm. The proportional relationship between increasing the GNP concentration and the peak intensities can be observed.

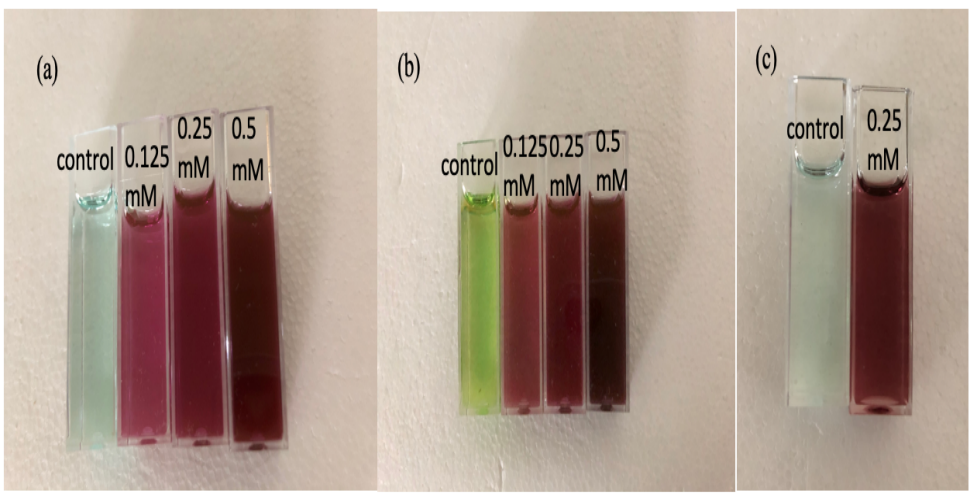

Figure 22. PRESAGE® cuvettes for (a) F1 and (b) F2 with 0.0, 0.125, 0.25, and 0.5 mM 50 nm GNPs, and (c) PRESAGE® cuvettes for F1 with 0.0 and 0.25 mM of 5 nm GNPs.

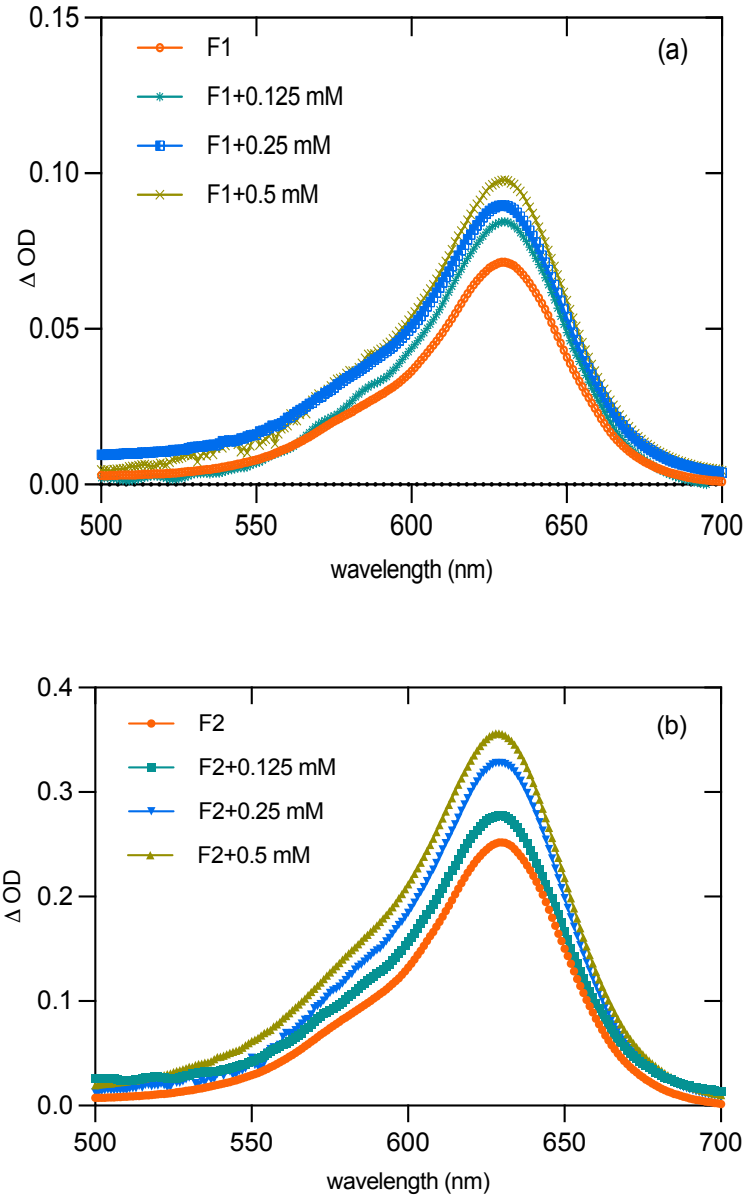

Figure 23. Absorption spectra of PRESAGE® dosimeter formulas (a) F1 and (b) F2 from 500-700 nm, showing absorbing maxima at around 630 nm after being irradiated to 10 Gy. The absorption was measured pre- and post-irradiation of obtained absorption measurements and Δ absorbance was calculated as their difference.

3.2.c. Calibration curve

The changes in measured maximum absorbance versus absorbed doses for all of the dosimeters are shown in Figure 24 (a), (b) for 150 kVp and (c), (d) for 6 MV radiation. An excellent linearity correlation ($R^2 > 0.99$) was observed over the investigated radiation dose range for all PRESAGE® formulas with and without GNPs. The sensitivities and R^2 values for all PRESAGE® dosimeters used in this study are also given in Figure 24. Where dose sensitivity is described as the slope of the dose and Δ absorbance in the optical density curve [16].

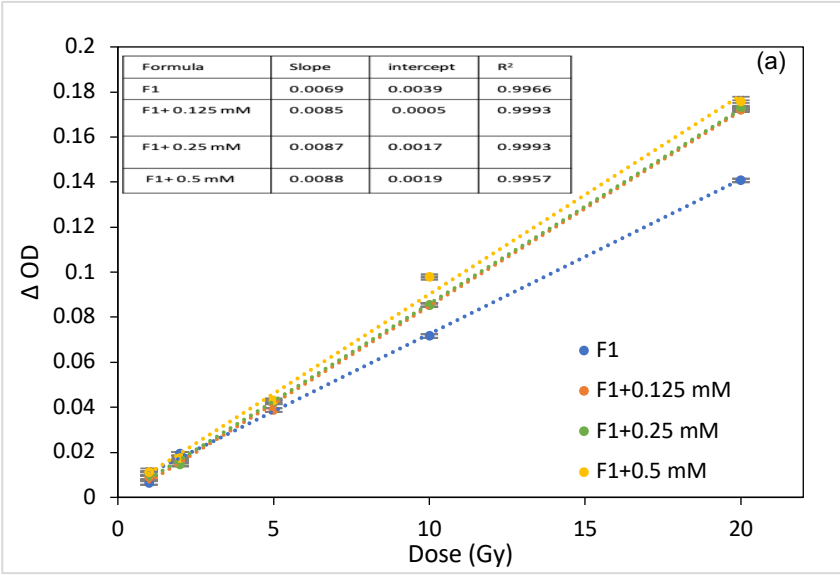
(a)
Formula | Slope | intercept | R²
F1 | 0.0069 | 0.0039 | 0.9966
F1+0.125 mM | 0.0085 | 0.0005 | 0.9993
F1+0.25 mM | 0.0087 | 0.0017 | 0.9993
F1+0.5 mM | 0.0088 | 0.0019 | 0.9957
Δ OD
Dose (Gy)
F1
F1+0.125 mM
F1+0.25 mM
F1+0.5 mM

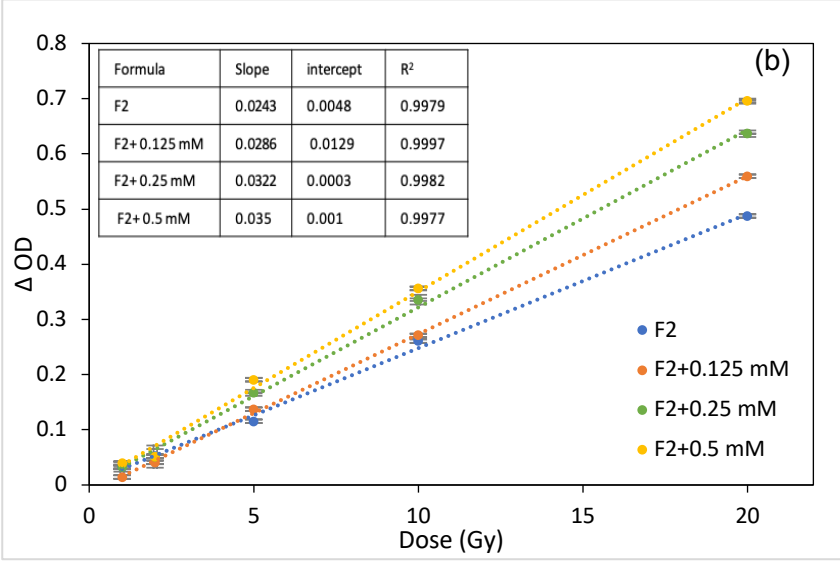
(b)
Formula | Slope | intercept | R²
F2 | 0.0243 | 0.0048 | 0.9979
F2+0.125 mM | 0.0286 | 0.0129 | 0.9997
F2+0.25 mM | 0.0322 | 0.0003 | 0.9982
F2+0.5 mM | 0.035 | 0.001 | 0.9977
Δ OD
Dose (Gy)
F2
F2+0.125 mM
F2+0.25 mM
F2+0.5 mM

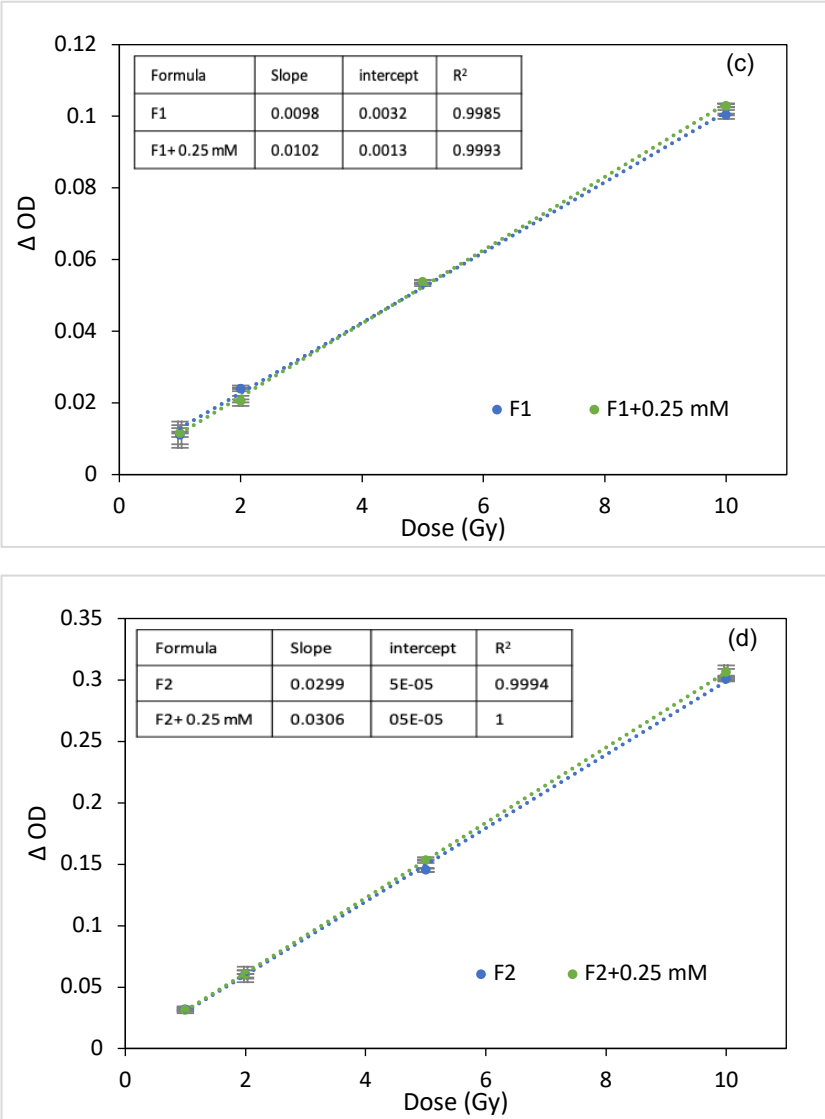

Figure 24. Absorbance changes as a function of absorbed radiation dose for PRESAGE® formula (a) F1 with 0.125, 0.25 and 0.5 mM of GNPs concentration and (b) F2 with 0.125, 0.25 and 0.5 mM of GNPs concentration. Which were fabricated in-house, showing the response at 150 kVp in (a), (b) and at 6 MV in (c) and (d) within 1 hour after irradiation. Error bars: ± standard deviation (n = 3).

Moreover, the linearity of the PRESAGE® formulas with the GNP concentration implies that the particles are dispersed into the dosimeter homogeneously. One component of the PRESAGE® is cyclohexanone, which is a cyclic ketone made up of cyclohexane with one oxo substituent [33]. In cyclohexane (nonpolar solvent), spherical GNPs with a specified size and narrow size distribution can be synthesized and may be employed directly in hybrid organic–inorganic devices, such as memory components or polymeric thin-film transistors [86]. This could suggest that using such solvents in PRESAGE® formulas embedded with GNPs may not contribute to any nanoparticle aggregation.

An abundance of surface atoms with delocalized electrons that exhibit plasmon wave behavior are what give GNPs their unique features. Donor–acceptor species, or ligands, can bond because the coordination sites of the surface atoms are not fully developed. As molecules join the nanoparticle surface in solution, a double layer of charge is created that inhibits the nanoparticles from aggregating [87]. Additionally, chemicals (coating agents) that “switch” the surface charge of GNPs from negatively charged to positively charged can be used to functionalize particles [87]. Polyvinylpyrrolidone (PVP), used in the current study, is a polymer with a lengthy polyvinyl backbone that is fully non-toxic and works well as a capping agent, particularly

for noble metal particles [88]. PVP is also known to be soluble in physiological solutions and water [88]. and it was found that, following 24 h of exposure,, 5 nm GNPs stabilized with PVP were easily absorbed by hepatocytes, kupffer cells, and blood vessel endothelial cells in vitro and in vivo. Consequently, hepatocytes did not show any evidence of toxicity [89].

The DEF was calculated as the ratio between the slope of the PRESAGE® dosimeter doped with GNPs and that without it. The calculated DEF shows different results among the two bromine-based PRESAGE® dosimeters. For formula F1, calculated DEF values were 1.23, 1.26, and 1.27 for the GNP concentrations of 0.125, 0.25, and 0.5 mM, respectively.

It should also be mentioned that a higher DEF (~ 1.6) for 0.5 mM was seen for only two batches. However, a DEF of 1.27 is shown for reproducibility.

For formula F2, the calculated DEFs were 1.20, 1.33, and 1.45 for GNP concentrations of 0.125, 0.25, and 0.5 mM, respectively. For the same GNP concentration of 0.125 mM, formula F1 shows a higher DEF than F2 by 2.5%. However, for the higher concentration of 0.25 and 0.5 mM, formula F2 indicated a higher DEF than F1 by 5.1% and 14%, respectively.

For the 6 MV radiation, both formulas F1 and F2 showed an

insignificant increase of the DEF by 4% and 2%, respectively. This small increase could be a result of the low-energy components of the Elekta 6 MV LINAC and its increase in electron density and cross sections [43].

To compare the measured DEFs with other published results, it should be emphasized that direct comparison could be irrelevant since there is variation in PRESAGE® components such as radical initiators, GNP type and size, and the energy spectra.

Alqathami et al. [69] used 0.5 mM of 50 nm GNPs with PRESAGE® and found the DEFs to be 1.77 and 1.11 for 100 kVP and 6 MV, respectively. Their finding for 6 MV was much higher than expectations.

On the other hand, Gagliardi et al. [43] reported DEFs using 50 nm GNPs and 0.25, 0.5 and 1 mM with PRESAGE® dosimeter and 150 kVp as 1.13, 1.14 and 1.16, respectively. The almost similar enhancement seen in their investigation, even though GNPs concentration increased, was also observed in our research with formula F1; DEF values were 1.23, 1.26, and 1.27 for the GNPs concentration of 0.125, 0.25, and 0.5 mM, respectively.

This could indicate that bromine-based PRESAGE® dosimeters (used in this study and in [69]) are a better match to the GNPs than chlorine-based PRESAGE® dosimeters (used in [43]). Radical

initiators are substances that can generate radical species under specific circumstances and encourage radical reactions. These substances often have covalent bonds that are weak or unstable and have low bond dissociation energies. Because these compounds have low bond dissociation energies, they are quickly broken down by heat or radiation, for example, resulting in the formation of free radical species [12]. The C-X bond dissociation energy (where X = Cl, Br, or I) and the quantity of free radicals generated are both directly related [90]. Due to the presence of an alkylbromide in Formulas F1 and F2, which is more radiation-sensitive than an alkylchloride, free radicals are produced more easily when exposed to ionizing radiation. This causes more LMG to be oxidized, which increases the optical density change [15].

Therefore, bromine-based PRESAGE® dosimeters showed higher radiation sensitivity than the chlorine-based dosimeters which is related to the higher dissociation energy of C-Cl bond 83.7 $kcal.mol^{-1}$ compared to 72.1 $kcal.mol^{-1}$ for C-Br bond [91]. As a result, the homolysis of bromine-based radical initiator requires less energy than the homolysis of chlorine-based radical initiator in order to produce free radicals [12]. The transmission of ionizing radiation's energy to a substance as it travels along its route is how ionizing radiation starts. Since secondary electrons are produced through photoelectric effect,

Compton scattering, and pair production, gamma and X-rays deposit the majority of their energy through these particles [12]. The presence of GNPs in PRESAGE® dosimeters with the combination of low energy radiation could enhance the radiation dose further as a result of the excessive number of low energy free radicals created by the increase of photoelectric interactions and the close proximity of their interaction products (photoelectrons, characteristic X-rays, and Auger electrons) [12], [41].

Furthermore, to investigate the GNP size effect on DEF, formula F1 was fabricated and 5 nm GNPs with concentration of 0.25 mM were incorporated into the F1 mixture.

Figure 25 shows the absorbance spectra versus absorbed dose for formula F1 loaded with 0.25 mM of either 5 nm or 50 nm GNPs. The DEF calculated for formula F1 with 0.25 mM of 5 nm GNPs was 1.6, which indicate a 29% higher DEF than the one with a larger GNP diameter of 50 nm.

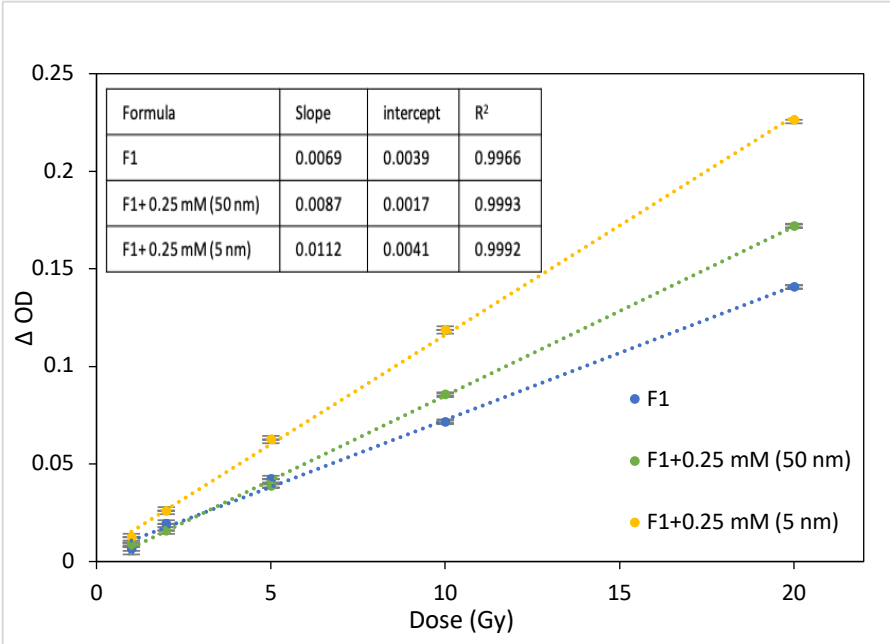

Figure 25. Absorbance changes as a function of absorbed radiation dose for PRESAGE® formula F1 with 0.25 mM of GNPs concentration and 5 nm and 50 nm diameter showing the response at 150 kVp in within 1 hour after irradiation. Error bars: ± standard deviation (n = 3).

This finding is in a good agreement with a reported DEF of 1.51, where they used 5 nm GNPs and an irradiation of 150 kVp as well [92]. Gagliardi et al. [43] studied 5 nm and 50 nm GNPs, 5–50 nm bismuth nanoparticles, and 80 nm bismuth nanoparticles at concentrations ranging from 0.25 mM to 2 mM and irradiated to various energies. The 95.3 keV mean energy synchrotron beam had the greatest dose enhancement (16–32%), then 150 kVp superficial beam (12–21%), and finally the 6 MV beam (2–5%). However, they reported no size dependency was observed for 5 nm GNPs and irradiated to 150 kVp, the DEFs were 1.13 for both sizes. This could be another indication of the dependency of DEFs on the PRESAGE® formula; the bromine-based PRESAGE® dosimeter showed higher DEFs compared to those with chlorine. Table 9 shows the inter-batch variability for formula F1 and F2 loaded with three GNP concentrations.

Table 9. Inter-batch variability for three batches and for each formula after exposure to 10 Gy with 150-kVp X-rays.

Formula	Batch	ΔOD	SD
F1 (0.125 mM)	1	0.079	0.00008
	2	0.083	0.00005
	3	0.085	0.00006
F1 (0.25 mM)	1	0.087	0.00089
	2	0.098	0.00044
	3	0.098	0.00046
F1 (0.5 mM)	1	0.096	0.00002
	2	0.100	0.00004
	3	0.084	0.00011
F2 (0.125 mM)	1	0.271	0.00060
	2	0.283	0.00007
	3	0.283	0.00009
F2 (0.25 mM)	1	0.320	0.00022
	2	0.336	0.00080
	3	0.325	0.00056
F2 (0.5 mM)	1	0.338	0.00052
	2	0.340	0.00270
	3	0.356	0.00086

Also, a lower concentration of the GNPs (0.025 mM) was investigated with the formula F2. The DEF showed only 4 % enhancement, which suggest that lower concentration can only produce a small enhancement. Figure 26 shows the absorbance change obtained as a function of different radiation doses.

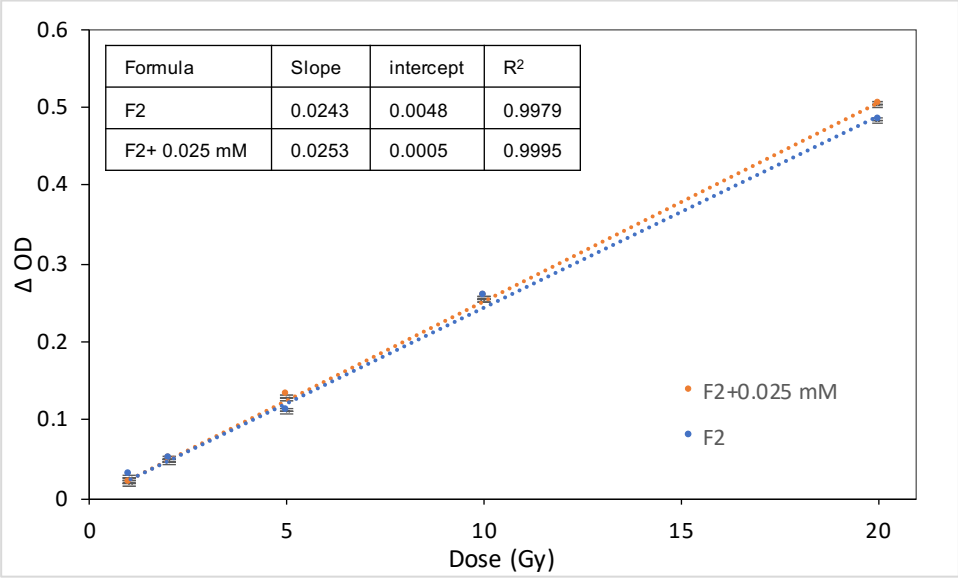

Figure 26. Absorbance changes as a function of absorbed radiation dose for PRESAGE® formula F2 with 0.025 mM of 50 nm GNPs concentration. Which were fabricated in-house, showing the response at 150 kVp in within 1 hour after irradiation. Error bars: ± standard deviation (n = 3).

3.2.d. Monte Carlo modeling

Table 10 summaries the DEFs results for 150 kVp and 6 MV irradiation compared with Monte Carlo simulations. In general, the results between DEFs calculated with Monte Carlo and the ones measured experimentally agrees within 5%.

The simulation underestimates the DEFs for the lowest GNPs concentration of 0.125 mM compared with experimental result for both formulas F1 and F2 by 8% and 18%, respectively.

This could be the result of the simulation of a homogenous mixture rather than the microscopic distribution of the GNPs, which could be more comparable to the experiment.

It also should be mentioned that the properties of GNPs vary significantly from the inert metallic form of the gold atom, which could affect the simulation results when compared to the experiment.

However, the simulation of 0.5 mM for formula F1 agrees more with the two batches, which had a DEF of 1.6 than the other batches of 1.27.

Also, the result of DEF for 5 nm GNPs simulation was 1.55 which agrees within 3% with the experiment.

For the 6 MV, the simulation underestimates the DEFs of 0.25 mM for formula F1 and F2 by only 5% and 2.2%, respectively.

Table 10. Dose enhancement factor at each energy and concentration for AuNPs with 50-nm diameter used in this study and compared with Monte Carlo simulation results. Uncertainty represent ± SD for three batches, relative errors*, ± SD for two cuvettes**.

Energy	PRESAGE Formula	Au molarity concentration	DEF simulation (± 0.0006-0.001)*	DEF experiment
150 kVp	F1	0.125 mM	1.13	1.23 ± 0.01
		0.25 mM	1.25	1.26 ± 0.02
		0.5 mM	1.50	1.27 ± 0.01
	F2	0.125 mM	1.013	1.20 ± 0.02
		0.25 mM	1.26	1.33 ± 0.03
		0.5 mM	1.51	1.45 ± 0.01
6 MV**	F1	0.25 mM	0.989	1.041 ± 0.03
	F2		1.000	1.023 ± 0.01

3.2.e. DEFs with GNPs concentration

It was observed that the dose enhancement was directly proportional to GNPs concentration. However, this increment was not linear with the GNPs concentration as shown in Figure 27. The reduced ability of the interaction to deposit energy further could be the cause of such non-linearity [43].

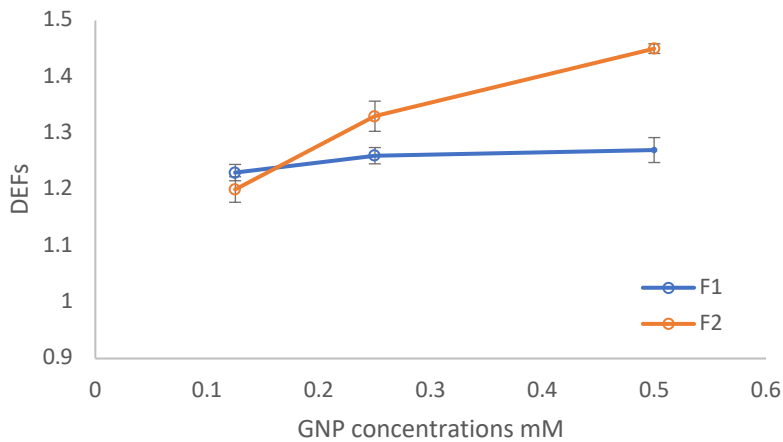

Figure 27. Relationship between DEFs and GNP concentrations of 0.125, 0.25 and 0.5 mM for formulas F1 and F2. Error bars: ± standard deviation (n = 3).

3.2.f. SEM and EDS of PRESAGE® dosimeter

Focused ion beam Scanning electron microscopy (SEM) (Helios 5 UC (FEI), Advance Institute Of Convergence Technology) was done for the solid PRESAGE®. In order to image it, smaller pieces of 1 × 1 × 3 mm slabs were prepared and cut with a machinery cutter. Figure 28 shows the SEM stage before (a) and after (b) acquiring the images. As shown in Figure 28 (b), the dosimeters look damaged after imaging.

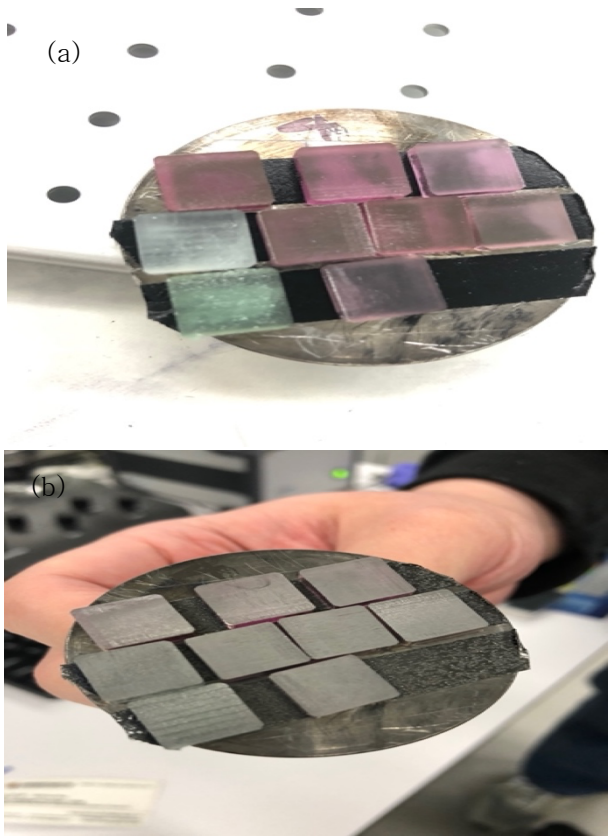

Figure 28. Images of PRESAGE samples in a slab shape mounted on the scanning electron microscope (SEM) stage (a) pre-imaging and (b) post-imaging.

Figures 29 and 30 show the SEM and energy-dispersive X-ray spectroscopy (EDS) images for PRESAGE® formulas F1 and F2 either with 0.25 mM 5 nm GNPs or 0.5 mM 50 nm GNPs. It was observed that even when using 10000 magnification, there was an internal melting of the PRESAGE® material which is caused by the electron beam hitting the samples. The melting created an internal disruption, leading to difficulty characterizing the exact GNPs size and distribution. However, EDS images and analysis were able to detect the GNPs and the other main components of PRESAGE® formulas F1 and F2. It should be mentioned that there are no publications with SEM images for PRESAGE® dosimeters as a whole formula; however, there are only SEM images of the GNPs that were used in their studies.

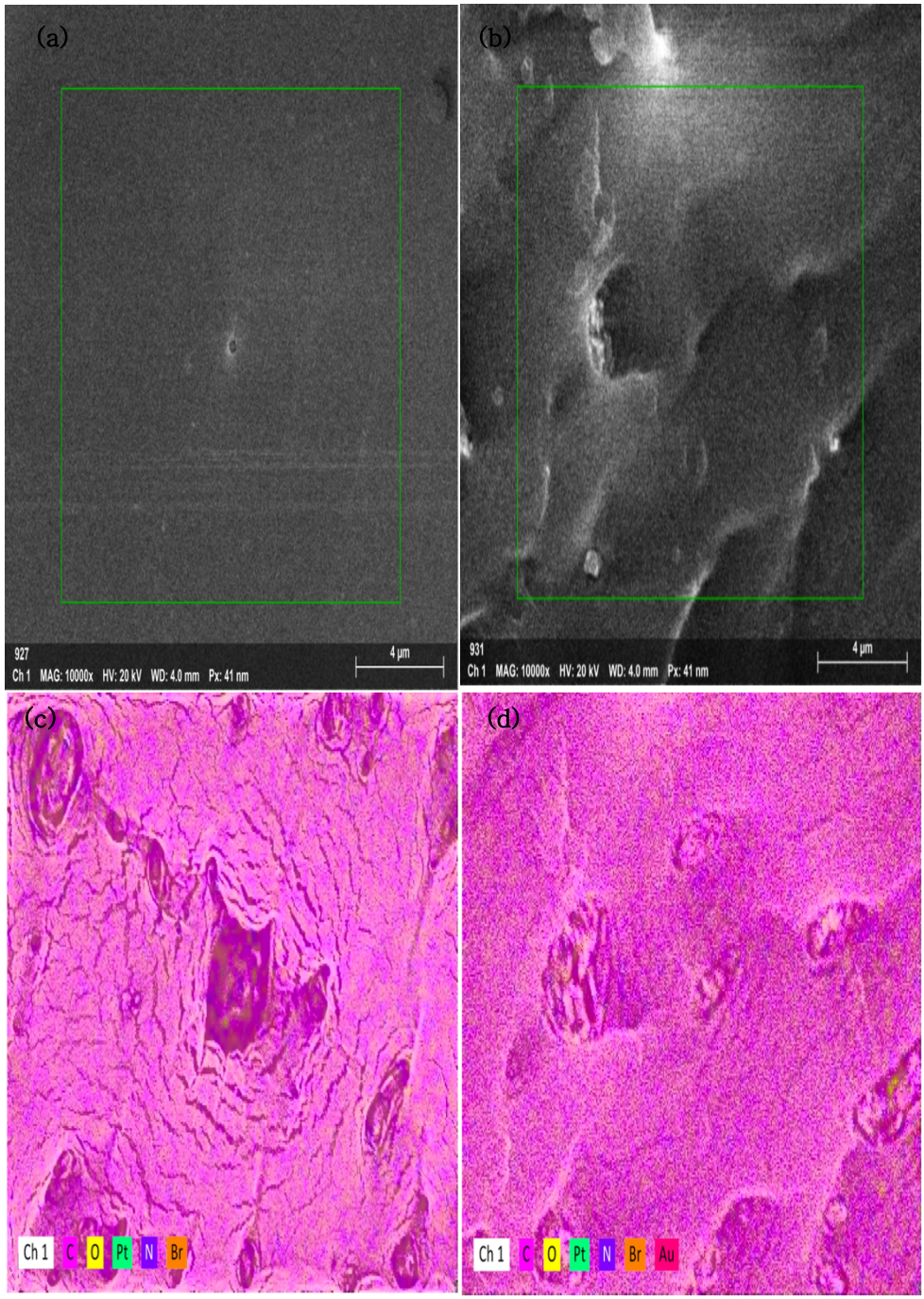

Figure 29. Scanning electron microscope (SEM) images of (a) formula F1 control and (b) formula F1 + 0.25 mM 5 nm GNPs. Energy-dispersive X-ray spectroscopy EDS of (c) formula F1 control and (d) F1 + 0.25 mM 5 nm GNPs; the main components of the dosimeter are detected and indicated.

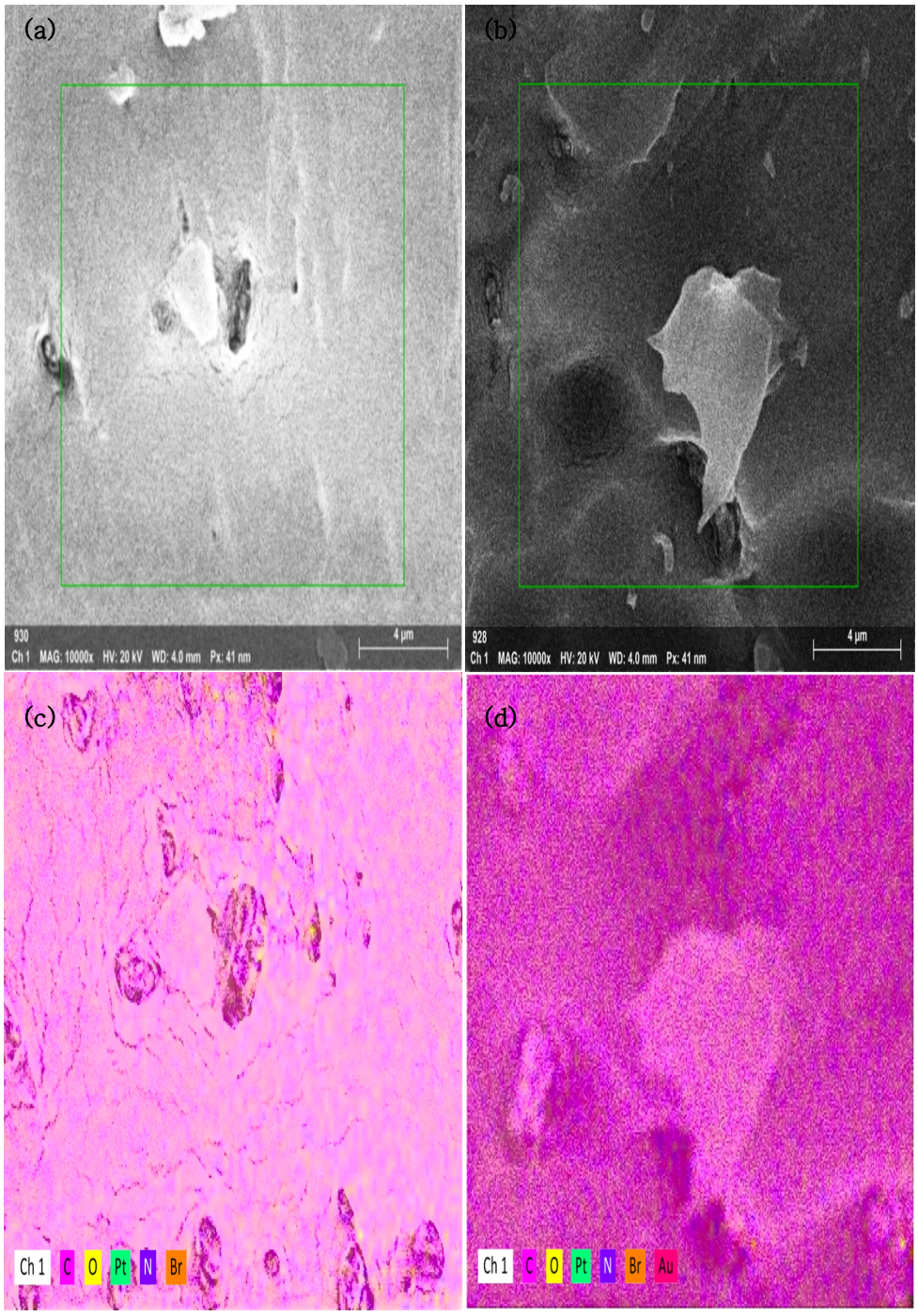

Figure 30. Scanning electron microscope (SEM) images of (a) formula F2 control and (b) formula F2 + 0.5 mM 50 nm GNPs. Energy-dispersive X-ray spectroscopy EDS of (c) formula F2 control and (d) F2 + 0.5 mM 50 nm GNPs; the main components of the dosimeter are detected and indicated.

3.3. Experimental uncertainties

In this experimental work, there are two types of errors that could occur. Experimental errors and statistical errors. The former may come from the experimental work, which include the fabrication steps of PRESAGE® dosimeter, irradiation and reading the cuvettes [9]. It has been noticed that there was a deviation in the weight percentage (wt.%) when measuring the chemicals of ± 0.5% which was also observed in a previous study [12].

The chemicals have to be stored according to their SDS, failure to do this could change their appearance and thus their properties. LMG was noticed to be a sensitive chemical and some bottles would have different purity levels that can be detected by eyes (i.e., color is different) which eventually could affect the uncertainty.

The accuracy of dose delivery by the X-rad was measured using an ionization chamber, for example, 1.0047 Gy (± 0.000019) was obtained for 100 kV and 1.0097 Gy (± 0.000104) for 150 kV.

For the spectrophotometer device, it was used with standard procedure and it was believed to be accurate since it has high resolution of 1 nm [12]. The data acquired for this experiment were for three measurements with the mean and standard deviation (unless it was stated otherwise).

3.4. DISCUSSION

In this study, enhancement of PRESAGE® dosimeter formulas was investigated and achieved for specific formulas. This includes formula-related sensitivity and dose enhancement due to GNPs. Several limitations were seen in this study, including; the absorption limit from the spectrophotometer (4 AU) in which the data cannot be recognized or measured above this certain value. This limits the range of GNPs concentration that could be incorporated into PRESAGE® dosimeter. Thus, there is a limit to detect the DEFs. Moreover, the PRESAGE® dosimeter can be really obscure if a higher concentration was used. The achieved absorbed dose enhancement may be restricted by cellular toxicity and cellular uptake, especially when investigating higher GNPs concentration than the ones studied here.

The possible toxicity when fabricating the PRESAGE® dosimeter that could impose health threats when care is not taken. Some of the dosimeters' components have been classified as dangerous chemicals (i.e., halocarbons) and protective measures such as protective eye wear, N masks, limiting the time of fabrication and using a hood are needed [93]. Cost-effectiveness should be taken into account before starting this study, high cost of some of the materials may cause limited trials.

3.5. CONCLUSIONS

In this investigation, we fabricated seven PRESAGE® dosimeters in-house for various applications. The addition of two solvents, cyclohexanone and DMSO, to two bromine-based radical initiators, CBr_4 and $C_2H_2Br_4$, was studied. When these two radical initiators were exposed to radiation, CBr_4 was more sensitive to it and released more free radicals. If high sensitivity is necessary, radical initiator (CBr_4) with PRESAGE® dosimeters can be employed.

When applying a greater quantity of radical initiator (0.50% wt.), however, the effective atomic number is not water-equivalent. At low doses (1 and 2 Gy), F6 and F7 displayed slight spectra changes, which might indicate that $C_2H_2Br_4$ is not stable as a radical initiator at such low doses.

The results show that formula F2 has a higher sensitivity and an effective atomic number close to water than other previously announced PRESAGE® formulas (with 0.49% difference). Furthermore, without taking into account correction factors, formula F2 may be employed in both kilovoltage and megavoltage beams based on depth-dose curves. The inclusion of DMSO to several of the formula has significantly improved their sensitivity and increased their Z_{eff}. Depending on the use of PRESAGE® dosimeters, a compromise

between required sensitivity and radiological characteristics should be addressed accordingly.

Also in this study, we have fabricated two bromine-based PRESAGE® dosimeters in-house with and without GNPs with different concentrations to investigate the physical dose enhancement and the effect of different PRESAGE® dosimeter formulas on the DEFs. Irradiation to superficial and megavoltage X-ray beams were done. Two bromine-based radical initiators CBr_4 and $C_2H_2Br_4$ were investigated with the addition of 50 nm GNPs, and 5 nm GNPs with $C_2H_2Br_4$.

Using similar concentrations (0.25 and 0.5 mM), the dose enhancement caused by the presence of GNPs in CBr_4-based PRESAGE® dosimeter was higher than $C_2H_2Br_4$-based PRESAGE® dosimeter for 150 kVp.

The increase in dose in F1 was up to 27% for 50 nm GNPs at the highest investigated concentration of 0.5 mM irradiated in 150 kVp and 45% in F2. While for 6 MV, the increase in dose was only 4% and 2% for F1 and F2, respectively.

For 5 nm GNP and 0.25 mM, the increase in dose was 60% measured by F1, which suggests the dependency of dose enhancement on GNP size.

The dose enhancement was directly proportional to GNP concentration but in a non-linear relationship.

Monte Carlo simulation showed good agreement with the GNPs concentration studied except for the underestimation of the lowest concentration of 0.125 mM GNPs.

The subsequent studies could be a continuation of this work;

Figure 31 shows incomplete research for PRESAGE® dosimeter fabricated in-house and shaped as human's parotid gland; this dosimeter could be used for field shaping with a lead frame cut-out for electron treatment in radiotherapy and measure the possible dose leakage to the surrounding healthy tissues.

Figure 31. PRESAGE® dosimeter fabricated in-house and shaped as a human parotid gland.

Another suggestion is to investigate the feasibility of using the Raman spectroscopy to read out the PRESAGE® sample and if possible

to detect the GNPs peak; Figure 32 shows a slab of PRESAGE® fabricated in-house with GNPs.

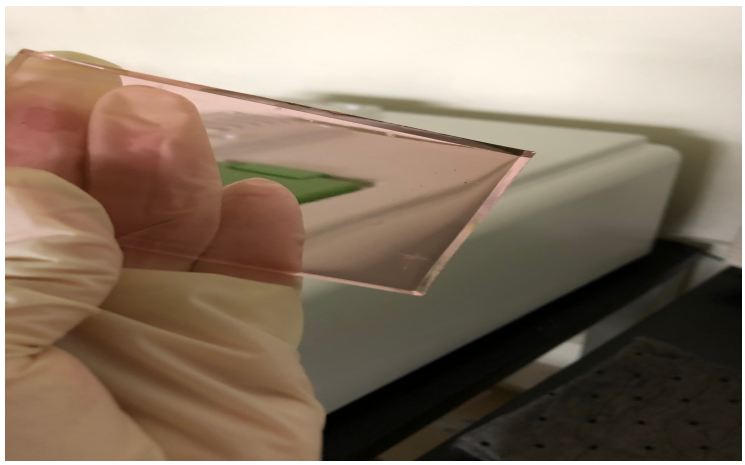

Figure 32. PRESAGE® dosimeter embedded with 50 nm GNPs and fabricated in slab form.

A worthwhile field of investigation is the possible toxicity that could emerge during the fabrication of the PRESAGE® dosimeter, which includes in-depth quantitative data.

Determining the best approach to image the nanoparticles distribution inside the PRESAGE® dosimeter is another challenging investigation.

REFERENCES

[1] F. Bray, J. Ferlay, I. Soerjomataram, R. L. Siegel, L. A. Torre, and A. Jemal, "Global cancer statistics 2018: GLOBOCAN estimates of incidence and mortality worldwide for 36 cancers in 185 countries," CA: A Cancer Journal for Clinicians, vol. 68, no. 6, pp. 394–424, Nov. 2018, doi: 10.3322/caac.21492.

[2] F. M. Khan, The physics of radiation therapy. Lippincott Williams & Wilkins, 2003.

[3] E. B. Podgorsak, "Radiation Oncology Physics: A Handbook for Teachers and Students". Vienna: International Atomic Energy Agency, 2005. [Online]. Available: http://www.iaea.org/books.

[4] C. Baldock et al., "Polymer gel dosimetry.," Phys Med Biol, vol. 55, no. 5, pp. R1–63, Mar. 2010, doi: 10.1088/0031-9155/55/5/R01.

[5] M. Sedaghat, R. Bujold, and M. Lepage, "Severe dose inaccuracies caused by an oxygen-antioxidant imbalance in normoxic polymer gel dosimeters," Physics in Medicine and Biology, vol. 56, no. 3, pp. 601–625, Feb. 2011, doi: 10.1088/0031-9155/56/3/006.

[6] R. J. Hernandez, S. E. M. Selke, and J. D. Culter, Plastics Packaging : Properties, Processing, Applications, and Regulations. Hanser Publishers, 2000.

[7] J. Adamovics and M. J. Maryanski, "Characterisation of PRESAGE™: A new 3-D radiochromic solid polymer dosemeter for ionising radiation," Radiation Protection Dosimetry, vol. 120, no. 1–4, pp. 107–112, 2006, doi: 10.1093/rpd/nci555.

[8] J. Adamovics, and J. Dietrich, "Enhanced Performance of PRESAGE - Sensitivity , and Post- Irradiation Stability," Med Phys, vol. 32, p. 1, 2005.

[9] J. Adamovics and M. J. Maryanski, "Characterisation of PRESAGE™: A new 3-D radiochromic solid polymer dosemeter for ionising radiation," Radiation Protection Dosimetry, vol. 120, no. 1–4, pp. 107–112, 2006, doi: 10.1093/rpd/nci555.

[10] T. Juang, R. Grant, J. Adamovics, G. Ibbott, and M. Oldham, "On the feasibility of comprehensive high-resolution 3D remote dosimetry," Medical Physics, vol. 41, no. 7, 071706, 2014, doi: 10.1118/1.4884018.

[11] M. Smith, J. March, and J. March, "March's Advanced Organic Chemistry : Reactions, Mechanisms, and Structure." Wiley, 2001.

[12] B. Mamdooh Alqathami, "Novel 3D Radiochromic Dosimeters for Advanced Radiotherapy Techniques.". Ph.D. Thesis, RMIT University, Australia, 2013.

[13] H. Sardon et al., "Organic acid-catalyzed polyurethane formation via a dual-activated mechanism: Unexpected preference of n-activation over o-activation of isocyanates," J Am Chem Soc, vol. 135, no. 43, pp. 16235–16241, Oct. 2013, doi: 10.1021/ja408641g.

[14] D. Khezerloo et al., "PRESAGE® as a solid 3-D radiation dosimeter: A review article," Radiation Physics and Chemistry, vol. 141, no. Jan., pp. 88–97, 2017, doi: 10.1016/j.radphyschem.2017.06.002.

[15] M. Alqathami, A. Blencowe, M. Geso, and G. Ibbott, "Characterization

of novel water-equivalent PRESAGE® dosimeters for megavoltage and kilovoltage x-ray beam dosimetry," Radiation Measurements, vol. 74, pp. 12–19, 2015, doi: 10.1016/j.radmeas.2015.02.002.

[16] A. Mostaar, B. Hashemi, M. H. Zahmatkesh, S. M. R. Aghamiri, and S. R. Mahdavi, "A basic dosimetric study of PRESAGE: The effect of different amounts of fabricating components on the sensitivity and stability of the dosimeter," Physics in Medicine and Biology, vol. 55, no. 3, pp. 903–912, 2010, doi: 10.1088/0031-9155/55/3/023.

[17] M. Alqathami, A. Blencowe, G. Qiao, J. Adamovics, and M. Geso, "Optimizing the sensitivity and radiological properties of the PRESAGE ® dosimeter using metal compounds," Radiation Physics and Chemistry, vol. 81, no. 11, pp. 1688–1695, 2012, doi: 10.1016/j.radphyschem.2012.06.004.

[18] M. Alqathami, A. Blencowe, G. Qiao, D. Butler, and M. Geso, "Optimization of the sensitivity and stability of the PRESAGE™ dosimeter using trihalomethane radical initiators," Radiation Physics and Chemistry, vol. 81, no. 7, pp. 867–873, 2012, doi: 10.1016/j.radphyschem.2012.03.022.

[19] S. Brown et al., "Radiological properties of the PRESAGE and PAGAT polymer dosimeters," Applied Radiation and Isotopes: Including Data, Instrumentation and Methods for Use in Agriculture, Industry and Medicine, vol. 66, no. 12, pp. 1970–1974, 2008, doi: 10.1016/j.apradiso.2008.06.005.

[20] Y. F. Wang, K. Liu, J. Adamovics, and C. S. Wuu, "An Investigation of dosimetric accuracy of a novel PRESAGE radiochromic sheet and its clinical applications." in Journal of Physics: Conference Series, vol. 1305, no. 1, Aug. 2019, doi: 10.1088/1742-6596/1305/1/012041.

[21] M. Dumas and J. T. Rakowski, "Sensitivity and variability of Presage dosimeter formulations in sheet form with application to SBRT and SRS QA," Medical Physics, vol. 42, no. 12, pp. 7138–7143, 2015, doi: 10.1118/1.4936104.

[22] Y. F. Wang, O. Dona, K. Liu, J. Adamovics, and C. S. Wuu, "Dosimetric characterization of a body-conforming radiochromic sheet," Journal of Applied Clinical Medical Physics, vol. 21, no. 3, pp. 167–177, Mar. 2020, doi: 10.1002/acm2.12838.

[23] E. Q. Youkahana, F. Gagliardi, and M. Geso, "Two-dimensional scanning of PRESAGE®dosimetry using UV/VIS spectrophotometry and its potential application in radiotherapy," Biomedical Physics and Engineering Express, vol. 2, no. 4, Jul., 2016, doi: 10.1088/2057-1976/2/4/045009.

[24] C. Collins, J. Kodra, S. W. Yoon, R. Coakley, J. Adamovics, and M. Oldham, "Preliminary investigation of a reusable radiochromic sheet for radiation dosimetry" in Journal of Physics: Conference Series, vol. 1305, no. 1, Aug. 2019, doi: 10.1088/1742-6596/1305/1/012032.

[25] N. Annabell, N. Yagi, K. Umetani, C. Wong, and M. Geso, "Evaluating the peak-to-valley dose ratio of synchrotron microbeams using PRESAGE fluorescence," Journal of Synchrotron Radiation, vol. 19, no. 3, pp. 332–339, May 2012, doi: 10.1107/S0909049512005237.

[26] L. J. Rankine et al., “Investigating end-to-end accuracy of image guided radiation treatment delivery using a micro-irradiator,” Physics in Medicine and Biology, vol. 58, no. 21, pp. 7791–7801, Nov. 2013, doi: 10.1088/0031-9155/58/21/7791.
[27] F. Costa, S. Doran, J. Adamovics, S. Nill, I. M. Hanson, and U. Oelfke, “Characterization of small PRESAGE® samples for measurements near the dosimeter edges,” in Journal of Physics: Conference Series, vol. 1305, no. 1, Aug. 2019, doi: 10.1088/1742-6596/1305/1/012009.
[28] L. Zhao, I. J. Das, Q. Zhao, A. Thomas, J. Adamovics, and M. Oldman, “Determination of the depth dose distribution of proton beam using PRESAGE^{TM} dosimeter,” in Journal of Physics: Conference Series, vol. 250, pp. 160–163, 2010, doi: 10.1088/1742-6596/250/1/012035.
[29] F. M. Gagliardi, R. D. Franich, and M. Geso, “Dose response and stability of water equivalent PRESAGE® dosimeters for synchrotron radiation therapy dosimetry,” Physics in Medicine and Biology, vol. 63, no. 23, Dec., 235027, 2018, doi: 10.1088/1361-6560/aaf1f5.
[30] S. Alghadhban, S. Youn, Y. Na, K. Kim, and S. J. Ye, “Optimization of bromine-based radical initiators using leucomalachite green and solvents in PRESAGE® dosimeter,” Radiation Physics and Chemistry, vol. 194, no. May, 2022, doi: 10.1016/j.radphyschem.2022.109985.
[31] S. Narasimha Murthy and H. N. Shivakumar, Topical and Transdermal Drug Delivery, first edit. Vitthal S. Kulkarni, 2009, doi: 10.1016/b978-0-8155-2025-2.10001-0.
[32] C. Jin, J. Chen, L. Yang, W. Luo, G. Wu, and Y. Zha, “Effect of DMSO on the sensitivity and diffusion of FPGX gel dosimeter,” Radiation Physics and Chemistry, vol. 81, no. 7, pp. 879–883, 2012, doi: 10.1016/j.radphyschem.2012.03.002.
[33] National Center for Biotechnology Information, “‘PubChem Compound Summary for CID 7967, Cyclohexanone’-PubChem,” PubChem, Available: https://pubchem.ncbi.nlm.nih.gov/compound/Cyclohexanone.
[34] Q. Ashton Acton, “Cyclohexanes : Advances in Research and Application,” 2012. doi: Available: http://ebookcentral.proquest.com/lib/snulibrary-ebooks/detail.action?docID=3403579.
[35] J. A. Adamovics, “Detection of therapeutic radiation in three-dimensions,” Beilstein Journal of Organic Chemistry, vol. 13, pp. 1325–1331, 2017, doi: 10.3762/bjoc.13.129.
[36] J. N. Duggan and C. B. Roberts, “Aggregation and precipitation of gold nanoparticle clusters in carbon dioxide-gas-expanded liquid dimethyl sulfoxide,” Journal of Physical Chemistry C, vol. 118, no. 26, pp. 14595–14605, Jul. 2014, doi: 10.1021/jp502151p.
[37] T. Juang, “Clinical Applications of 3D Dosimetry,” 2015, doi: Available: https://dukespace.lib.duke.edu/dspace/handle/10161/10478.
[38] T. Juang, R. Grant, J. Adamovics, G. Ibbott, and M. Oldham, “On the feasibility of comprehensive high-resolution 3D remote dosimetry,” Medical Physics, vol. 41, no. 7, pp. 1–11, 2014, doi: 10.1118/1.4884018.
[39] M. Kurudirek, “Studies on heavy charged particle interaction, water

equivalence and Monte Carlo simulation in some gel dosimeters, water, human tissues and water phantoms," Nuclear Instruments and Methods in Physics Research Section A: Accelerators, Spectrometers, Detectors and Associated Equipment, vol. 795, pp. 239–252, 2015, doi: 10.1016/j.nima.2015.06.001.

[40] T. Gorjiara et al., "Investigation of radiological properties and water equivalency of PRESAGE® dosimeters," Medical Physics, vol. 38, no. 4, pp. 2265–2274, 2011, doi: 10.1118/1.3561509.

[41] Y. Chen, J. Yang, S. Fu, and J. Wu, "Gold nanoparticles as radiosensitizers in cancer radiotherapy," International Journal of Nanomedicine, Dove Medical Press Ltd, vol. 15, pp. 9407–9430, 2020, doi: 10.2147/IJN.S272902.

[42] M. Misawa and J. Takahashi, "Generation of reactive oxygen species induced by gold nanoparticles under x-ray and UV Irradiations," Nanomedicine: Nanotechnology, Biology, and Medicine, vol. 7, no. 5, pp. 604–614, Oct. 2011, doi: 10.1016/j.nano.2011.01.014.

[43] F. M. Gagliardi, R. D. Franich, and M. Geso, "Nanoparticle dose enhancement of synchrotron radiation in PRESAGE dosimeters," Journal of Synchrotron Radiation, vol. 27, no. 6, pp. 1590–1600, Nov. 2020, doi: 10.1107/S1600577520012849.

[44] W. N. Rahman et al., "Enhancement of radiation effects by gold nanoparticles for superficial radiation therapy," Nanomedicine: Nanotechnology, Biology, and Medicine, vol. 5, no. 2, pp. 136–142, Jun. 2009, doi: 10.1016/j.nano.2009.01.014.

[45] R. E. Serda, B. Godin, E. Blanco, C. Chiappini, and M. Ferrari, "Multi-stage delivery nano-particle systems for therapeutic applications," Biochimica et Biophysica Acta, vol. 1810, no. 3, pp. 317–329, Mar. 2011, doi: 10.1016/j.bbagen.2010.05.004.

[46] W. N. Rahman, C. J. Wong, T. Ackerly, N. Yagi, and M. Geso, "Polymer gels impregnated with gold nanoparticles implemented for measurements of radiation dose enhancement in synchrotron and conventional radiotherapy type beams," Australasian Physical and Engineering Sciences in Medicine, vol. 35, no. 3, pp. 301–309, 2012, doi: 10.1007/s13246-012-0157-x.

[47] S. Jain et al., "Cell-Specific Radiosensitization by gold nanoparticles at megavoltage radiation energies," International Journal of Radiation Oncology, Biology, Physics, vol. 79, no. 2, pp. 531–539, Feb. 2011, doi: 10.1016/j.ijrobp.2010.08.044.

[48] K. T. Butterworth, S. J. McMahon, F. J. Currell, and K. M. Prise, "Physical basis and biological mechanisms of gold nanoparticle radiosensitization," Nanoscale, vol. 4, no. 16, pp. 4830–4838, Aug. 2012, doi: 10.1039/c2nr31227a.

[49] S. Penninckx, A. C. Heuskin, C. Michiels, and S. Lucas, "Gold nanoparticles as a potent radiosensitizer: A transdisciplinary approach from physics to patient," Cancers, MDPI, vol. 12, no. 8, pp. 1–361, Aug. 01, 2020, doi: 10.3390/cancers12082021.

[50] W. Seong, "Monte Carlo Simulations and Experiments of Metal Nanoparticle Enhanced Low-Energy Radiotherapy." Seoul National

University, 2018.
[51] J. C. Polf, L. F. Bronk, W. H. P. Driessen, W. Arap, R. Pasqualini, and M. Gillin, “Enhanced relative biological effectiveness of proton radiotherapy in tumor cells with internalized gold nanoparticles,” Applied Physics Letters, vol. 98, no. 19, May, 193702, 2011, doi: 10.1063/1.3589914.
[52] D. B. Chithrani et al., “Gold nanoparticles as radiation sensitizers in cancer therapy,” Radiation Research, vol. 173, no. 6, pp. 719–728, Jun. 2010, doi: 10.1667/RR1984.1.
[53] D. Y. Joh et al., “Selective targeting of brain tumors with gold nanoparticle–induced radiosensitization,” PLOS ONE, vol. 8, no. 4, Apr., e62425, 2013, doi: 10.1371/journal.pone.0062425.
[54] J. F. Hainfeld, D. N. Slatkin, and H. M. Smilowitz, “The use of gold nanoparticles to enhance radiotherapy in mice,” Physics in Medicine and Biology, vol. 49, no. 18, Sep., N309–N315, 2004, doi: 10.1088/0031-9155/49/18/N03.
[55] S. Liu et al., “Radiosensitizing effects of different size bovine serum albuminlated gold nanoparticles on H22 hepatoma-bearing mice,” Nanomedicine, vol. 13, no. 11, pp. 1371–1383, Jun., 2018, doi: 10.2217/nnm-2018-0059.
[56] Y. Dou et al., “Size-tuning ionization to optimize gold nanoparticles for simultaneous enhanced CT imaging and radiotherapy,” ACS Nano, vol. 10, no. 2, pp. 2536–2548, Feb. 2016, doi: 10.1021/acsnano.5b07473.
[57] T. Guo, “Physical, chemical and biological enhancement in X-ray nanochemistry,” Physical Chemistry Chemical Physics: PCCP, vol. 21, no. 29, pp. 15917–15931, 2019, doi: 10.1039/c9cp03024g.
[58] S. A. H. Alan Martin, “An Introduction To Radiation Protection.” Springer New York, NY, 1996. doi: https://doi.org/10.1007/978-1-4899-4543-3.
[59] K. T. Butterworth, S. J. McMahon, L. E. Taggart, and K. M. Prise, “Radiosensitization by gold nanoparticles: Effective at megavoltage energies and potential role of oxidative stress,” Translational Cancer Research, vol. 2, no. 4, pp. 269–279, Aug. 2013, doi: 10.3978/j.issn.2218-676X.2013.08.03.
[60] L. Cui, S. Her, G. R. Borst, R. G. Bristow, D. A. Jaffray, and C. Allen, “Radiosensitization by gold nanoparticles: Will they ever make it to the clinic?,” Radiotherapy and Oncology: Journal of the European Society for Therapeutic Radiology and Oncology. Elsevier Ireland Ltd, vol. 124, no. 3, pp. 344–356, Sep. 01, 2017, doi: 10.1016/j.radonc.2017.07.007.
[61] M. Douglass, E. Bezak, and S. Penfold, “Monte Carlo investigation of the increased radiation deposition due to gold nanoparticles using kilovoltage and megavoltage photons in a 3D randomized cell model,” Medical Physics, vol. 40, no. 7, 2013, doi: 10.1118/1.4808150.
[62] M. Douglass, E. Bezak, and S. Penfold, “Monte Carlo investigation of the increased radiation deposition due to gold nanoparticles using kilovoltage and megavoltage photons in a 3D randomized cell model,” Medical Physics, vol. 40, no. 7, 2013, doi: 10.1118/1.4808150.
[63] T. Gray et al., “A detailed experimental and Monte Carlo analysis of

gold nanoparticle dose enhancement using 6 MV and 18 MV external beam energies in a macroscopic scale," Applied Radiation and Isotopes: Including Data, Instrumentation and Methods for Use in Agriculture, Industry and Medicine, vol. 171, no. May, 109638, 2021, doi: 10.1016/j.apradiso.2021.109638.

[64] K. P. Chatzipapas et al., "Ionizing radiation and complex dna damage: Quantifying the radiobiological damage using Monte Carlo simulations," Cancers, vol. 12, no. 4. MDPI AG, Apr. 01, 2020, doi: 10.3390/cancers12040799.

[65] R. Liu, T. Zhao, X. Zhao, and F. J. Reynoso, "Modeling gold nanoparticle radiosensitization using a clustering algorithm to quantitate DNA double-strand breaks with mixed-physics Monte Carlo simulation," Medical Physics, vol. 46, no. 11, pp. 5314–5325, Nov. 2019, doi: 10.1002/mp.13813.

[66] B. Zh, K. H. R, and R. Zohdiaghdam, "Evaluation of Gold Nanoparticle Size Effect on Dose Enhancement Factor in Megavoltage Beam Radiotherapy Using MAGICA Polymer Gel Dosimeter,". 2019 [Online]. Available: www.jbpe.org

[67] B. D. Chithrani, A. A. Ghazani, and W. C. W. Chan, "Determining the size and shape dependence of gold nanoparticle uptake into mammalian cells," Nano Letters, vol. 6, no. 4, pp. 662–668, Apr. 2006, doi: 10.1021/nl052396o.

[68] F. Osaki, T. Kanamori, S. Sando, T. Sera, and Y. Aoyama, "A quantum dot conjugated sugar ball and its cellular uptake. On the size effects of endocytosis in the subviral region," J Am Chem Soc, vol. 126, no. 21, pp. 6520–6521, Jun. 2004, doi: 10.1021/ja048792a.

[69] M. Alqathami, A. Blencowe, U. J. Yeo, S. J. Doran, G. Qiao, and M. Geso, "Novel multicompartment 3-dimensional radiochromic radiation dosimeters for nanoparticle-enhanced radiation therapy dosimetry," International Journal of Radiation Oncology Biology Physics, vol. 84, no. 4, Nov., e549–e555, 2012, doi: 10.1016/j.ijrobp.2012.05.029.

[70] [edited by] Robert E Lenga, "The Sigma-Aldrich Library of Chemical Safety Data". ed. 2. [Milwaukee, Wis., USA] : Sigma-Aldrich Corp., [1988] 1988. [Online]. Available: https://search.library.wisc.edu/catalog/999610513502121.

[71] S. R. Manohara, S. M. Hanagodimath, K. S. Thind, and L. Gerward, "On the effective atomic number and electron density: A comprehensive set of formulas for all types of materials and energies above 1 keV," Nuclear Instruments and Methods in Physics Research Section B: Beam Interactions with Materials and Atoms, vol. 266, no. 18, pp. 3906–3912, Sep. 2008, doi: 10.1016/j.nimb.2008.06.034.

[72] J. Hubbell and S. Seltzer, "Tables of X-ray Mass Attenuation Coefficients and Mass Energy-Absorption Coefficients 1 keV to 20 MeV for Elements Z = 1 to 92 and 48 Additional Substances of Dosimetric Interest,". 1995.

[73] J. S. Taurozzi, V. A. Hackley, and M. R. Wiesner, "Preparation of Nanoparticle Dispersions from Powdered Material Using Ultrasonic Disruption-Version 1.1,", Jun. 2012, doi: 10.6028/NIST.SP.1200-2.

[74] J. F. Hainfeld, M. J. O'Connor, F. A. Dilmanian, D. N. Slatkin, D. J. Adams, and H. M. Smilowitz, "Micro-CT enables microlocalisation and quantification of Her2-targeted gold nanoparticles within tumour regions," British Journal of Radiology, vol. 84, no. 1002, pp. 526–533, Jun. 2011, doi: 10.1259/bjr/42612922.
[75] Y. P. Jia, B. Y. Ma, X. W. Wei, and Z. Y. Qian, "The in vitro and in vivo toxicity of gold nanoparticles," Chinese Chemical Letters, vol. 28, no. 4, pp. 691–702, 2017, doi: 10.1016/j.cclet.2017.01.021.
[76] G. Currell and D. G. Currell, Analytical instrumentation : Performance characteristics and quality. New York, UNITED KINGDOM: John Wiley & Sons, Incorporated, 2000. [Online]. Available: http://ebookcentral.proquest.com/lib/snulibrary-ebooks/detail.action?docID=470500. New York, United Kingdom: John Wiley & Sons, Inc.
[77] C. Burgess, "The basis for good spectrophotometric UV–visible measurements," in "UV-Visible Spectrophotometry of Waters and Soils." Elsevier, 2022, pp. 25–58. doi: 10.1016/B978-0-323-90994-5.00014-9.
[78] T. Goorley et al., Initial MCNP6 Release Overview. Nuclear Technology, vol. 180, no. 3, pp. 298–315, 2012.
[79] John. Dagpunar, "Simulation and Monte Carlo : With Applications in Finance and MCMC." John Wiley, 2007.
[80] G. Poludniowski, G. Landry, F. Deblois, P. M. Evans, and F. Verhaegen, "SpekCalc: A program to calculate photon spectra from tungsten anode x-ray tubes," Physics in Medicine and Biology, vol. 54, no. 19, N433–N438, 2009, doi: 10.1088/0031-9155/54/19/N01.
[81] C. J. Werner et al., "MCNP Version 6.2 Release Notes." United States, 2018, doi: 10.2172/1419730.
[82] D. Sheikh-Bagheri and D. W. O. Rogers, "Monte Carlo calculation of nine megavoltage photon beam spectra using the BEAM code," Medical Physics, vol. 29, no. 3, pp. 391–402, 2002, doi: 10.1118/1.1445413.
[83] A. M. El-Khayatt, "Water equivalence of some 3D dosimeters: A theoretical study based on the effective atomic number and effective fast neutron removal cross section," Nuclear Science and Techniques, vol. 28, no. 12, Dec., 2017, doi: 10.1007/s41365-017-0322-8.
[84] S. Brown et al., "Radiological properties of the PRESAGE and PAGAT polymer dosimeters," Applied Radiation and Isotopes: Including Data, Instrumentation and Methods for Use in Agriculture, Industry and Medicine, vol. 66, no. 12, pp. 1970–1974, Dec. 2008, doi: 10.1016/j.apradiso.2008.06.005.
[85] J. D. Cho et al., "Improvement in sensitivity of radiochromic 3D dosimeter based on rigid polyurethane resin by incorporating tartrazine," PLOS ONE, vol. 15, no. 3, e0230410, 2020, doi: 10.1371/journal.pone.0230410.
[86] K. Soliwoda et al., "Synthesis of monodisperse gold nanoparticles via electrospray-assisted chemical reduction method in cyclohexane," Colloids and Surfaces Part A: Physicochemical and Engineering Aspects, vol. 482, pp. 148–153, Oct. 2015, doi:

10.1016/j.colsurfa.2015.04.040.
[87] C. Daruich De Souza, B. Ribeiro Nogueira, and M. E. C. M. Rostelato, “Review of the methodologies used in the synthesis gold nanoparticles by chemical reduction,” Journal of Alloys and Compounds. Elsevier Ltd, vol. 798, pp. 714–740, Aug. 25, 2019, doi: 10.1016/j.jallcom.2019.05.153.
[88] T. Das, V. Kolli, S. Karmakar, and N. Sarkar, “Functionalisation of polyvinylpyrrolidone on gold nanoparticles enhances its anti-amyloidogenic propensity towards hen egg white lysozyme,” Biomedicines , vol. 5, no. 2. 2017, doi: 10.3390/biomedicines5020019.
[89] A. Sani, C. Cao, and D. Cui, “Toxicity of gold nanoparticles (AuNPs): A review,” Biochemistry and Biophysics Reports, vol. 26. Elsevier B.V., 100991, Jul. 01, 2021. doi: 10.1016/j.bbrep.2021.100991.
[90] J. A. Adamovics, “Detection of therapeutic radiation in three-dimensions,” no. Scheme 1, pp. 1325–1331, 2017, doi: 10.3762/bjoc.13.129.
[91] S. J. Blanksby and G. B. Ellison, “Bond dissociation energies of organic molecules,” Accounts of Chemical Research, vol. 36, no. 4, pp. 255–263, Apr. 2003, doi: 10.1021/ar020230d.
[92] M. Alqathami, A. Blencowe, M. Geso, and G. Ibbott, “Quantitative 3D determination of radiosensitization by bismuth-based nanoparticles,” Journal of Biomedical Nanotechnology, vol. 12, no. 3, pp. 464–471, Mar. 2016, doi: 10.1166/jbn.2016.2183.
[93] E. R. Kinkead et al., “The determination of the repeated oral toxicity of halocarbon oil, series 27-S,” Toxicology and Industrial Health, vol. 6, no. 1, pp. 17–32, Jan. 1990, doi: 10.1177/074823379000600102.
[94] V. , N. O. Make and I. T. Mistake ’ S UV THAT EVERYONE CAN USE.” [Online]. Solutions, “Lambda TM. Available: www.perkinelmer.com/UVVisSolutions vols. 265/365, no. 465.

Abstract

선량계측에서는 대부분의 방사선 치료가 회기당 저선량과 조직 등가특성을 사용하므로 보정인자가 필요하지 않기 때문에 방사선량계는 특히 저선량에서 높은 감도를 갖는 것이 바람직합니다. 방사선 선량계에 대해 고려해야 할 또 다른 요소는 필요한 선량을 전달하기 위해 높은 선량 기울기를 포함할 수 있는 고급 치료 기술에 대한 치료 계획을 검증하기 위해 선량을 3D로 측정하는 능력입니다. 이러한 검증및 품질 보증은 위험에 처한 중요 장기에 원치 않는 치사 방사선량을 유발할 수 있으므로 절대적으로 중요합니다. 다양한 목적으로 사용될 수 있는 선량계 공식에 대한 조사는 개발이 가능한 지속적인 연구영역이었습니다. 위험에 처한 주변 장기에 대한 방사선량을 최소화하면서 전달되는 방사선량을 향상시키기 위해 적용될 수 있는 또 다른 접근법은 높은 원자 번호의 나노 입자를 사용하는 것입니다. 이러한 나노입자가 탑재된 조직 등가선량계의 실험적 조사는 방사선 에너지의 가능한 의존성, 선량계의 구성요소 및 공식, 나노입자 크기효과 및 농도에 대한 자세한 정보를 제공할 수 있습니다.

따라서 본 연구는 크게 세 가지 목적을 가지고 있습니다. 첫 번째 목표는 더 높은 감도와 조직과 같은 등가 특성을 가진 이상적인 선량계를 개발하는 것입니다. F1 및 F2로 명명된 공식은 이 특정 목적을 위해 제작되었습니다. 두 번째 목적은 두 가지 브롬 기반 라디칼 개시제와두 가지 다른 용매 유형을 PRESAGE® 공식에 추가하는 것이 PRESAGE® 선량계의 방사선학적 특성

과 선량 감도에 미치는 영향을 결정하는 것입니다. F3, F4, F5, F6, F7으로 명명된 공식이 이 조사를 위해 조작되었습니다. tetrabromomethane (CBr_4) 및 1,1,1,2-tetrabromoethane ($C_2H_2Br_4$) 라디칼 개시제가 최대 2 wt.% 총 7개의 별개의 PRESAGE® 선량계 제작에 사용되었습니다. 그들은 0에서 40Gy의 선량 범위로 250 또는 100 kVp X선 방사선을 받았습니다. 분광 광도계를 사용하여 노출 전후의 광학 밀도 변화를 감지했습니다. 또한, DMSO (Dimethyl sulfoxide)의 함량은 2wt.%인 반면, 다양한 농도의 라디칼 개시제와 cyclohexanone에 대해PRESAGE® 선량계의 방사선학적 특성과 민감도를 조사했습니다. PRESAGE®/water 상대 깊이 선량과 다양한 X선 빔과 코발트-60에 대한 에너지 의존성을 몬테카를로 방법을 사용하여 연구했습니다.

세 번째 목표는 생물학적 강화와 상관없이 사내에서 제작된PRESAGE® 공식에서 높은 Z GNP의 물리적 용량 강화 영향을 평가하고 강화된 특성을 조사하는 것입니다. 실험 결과를 비교하기 위해 Monte Carlo 시뮬레이션을 수행했습니다.

첫 번째 목표에 대한 결과는 제작된 사내 PRESAGE® 선량계 공식F1 및 F2가 공식 F2를 사용하여 방사선에 다르게 반응하는 것이 조직 등가 특성을 동반한 MOD3으로 명명된 이전에 발표된 PRESAGE® 선량계 공식보다 방사선에 대한 감도가 개선되었음을 보여주었습니다. 또한 깊이 선량 응답에 대한 몬테카를로 시뮬레이션은 F2가 보정 계수에 대한 요구 사항 없이 킬로

및 메가전압빔 모두에 사용될 수 있음을 확인했습니다.

두 번째 목적에 대한 결과는 PRESAGE® 선량계 공식이 더 높은 감도를 얻기 위해 다른 화학 성분으로 제작될 수 있음을 보여주었습니다. 예를 들어, 혼합물에 디메틸 설폭사이드(DMSO)가 포함된 화학식 F5는 비 DMSO 공식과 비교하여 유효 원자 번호가 1%만 증가하면서 감도가 46% 증가함을 나타냅니다. 또한 Monte Carlo 시뮬레이션은 이러한 공식이 선량 측정 보정 계수 없이 메가전압 빔에 사용될 수 있는 반면 킬로전압 빔에는 보정이 필요함을 보여주었습니다. 더욱이, 라디칼 개시제로 tetrabromomethane을 갖는 화학식은 1,1,1,2-tetrabromoethane보다 더 높은 감도를 나타내었습니다.

세 번째 목표는 빔 에너지, GNP 크기 및 농도, PRESAGE® 선량계공식에 따라 현저한 선량 향상을 나타내는 조직 등가 PRESAGE® 선량계에 금 나노입자를 통합하여 달성되었습니다. 분명히 이 조사는 PRESAGE® 공식에 대한 의존성을 포함하여 용량 증가 결과에 영향을 미칠 수 있는 요인에 대한 이해를 제공합니다. 결과에 따르면 브롬 기반 PRESAGE® 선량계는 염소계보다 훨씬 더 높은 DEF를 나타냅니다.

첫 번째 목표에 대한 결과는 제작된 사내 PRESAGE® 선량계 공식F1 및 F2가 공식 F2를 사용하여 방사선에 다르게 반응하는 것이 조직 등가 특성을 동반한 MOD3으로 명명된 이전에 발표된 PRESAGE® 선량계 공식보다 방사

선에 대한 감도가 개선되었음을 보여주었습니다. 또한 깊이 선량 응답에 대한 몬테카를로 시뮬레이션은 공식 F2가 보정 계수에 대한 요구 사항 없이 킬로 및 메가전압빔 모두에 사용될 수 있음을 확인했습니다.

두 번째 목적에 대한 결과는 PRESAGE® 선량계 공식이 더 높은 감도를 얻기 위해 다른 화학 성분으로 제작될 수 있음을 보여주었습니다. 예를 들어, 혼합물에 디메틸 설폭사이드 (DMSO)가 포함된 화학식 F5는 비 DMSO 공식과 비교하여 유효 원자 번호가 1%만 증가하면서 감도가 46% 증가함을 나타냅니다. 또한 Monte Carlo 시뮬레이션은 이러한 공식이 선량 측정 보정 계수 없이 메가전압 빔에 사용될 수 있는 반면 킬로전압 빔에는 보정이 필요함을 보여주었습니다. 더욱이, 라디칼 개시제로 tetrabromomethane을 갖는 화학식은 1,1,1,2-tetrabromoethane보다 더 높은 감도를 나타내었습니다.

세 번째 목표는 빔 에너지, GNP 크기 및 농도, PRESAGE® 선량계공식에 따라 현저한 선량 향상을 나타내는 조직 등가 PRESAGE® 선량계에 금 나노입자를 통합하여 달성되었습니다. 분명히 이 조사는 PRESAGE® 공식에 대한 의존성을 포함하여 용량 증가 결과에 영향을 미칠 수 있는 요인에 대한 이해를 제공합니다. 결과에 따르면 브롬 기반 PRESAGE® 선량계는 염소계보다 훨씬 더 높은 DEF를 나타냅니다.